IBEX: A versatile multiplex optical imaging approach for deep phenotyping and spatial analysis of cells in complex tissues

Andrea J. Radtke[a,1,2], Evelyn Kandov[b,c,1], Bradley Lowekamp[d], Emily Speranza[b,e], Colin J. Chu[b], Anita Gola[b,f], Nishant Thakur[b], Rochelle Shih[b,f], Li Yao[g], Ziv Rafael Yaniv[d], Rebecca T. Beuschel[a], Juraj Kabat[h], Joshua Croteau[i], Jeremy Davis[j], Jonathan M. Hernandez[j], and Ronald N. Germain[a,b,2]

[a]Center for Advanced Tissue Imaging, Laboratory of Immune System Biology, National Institute of Allergy and Infectious Diseases, NIH, Bethesda, MD 20892; [b]Lymphocyte Biology Section, Laboratory of Immune System Biology, National Institute of Allergy and Infectious Diseases, NIH, Bethesda, MD 20892; [c]Department of Pharmacology, Vanderbilt University School of Medicine, Nashville, TN 37240; [d]Bioinformatics and Computational Bioscience Branch, National Institute of Allergy and Infectious Diseases, NIH, Bethesda, MD 20892; [e]Innate Immunity and Pathogenesis Section, Laboratory of Virology, National Institute of Allergy and Infectious Diseases, NIH, Hamilton, MT 59840; [f]The Rockefeller University, New York, NY 10065; [g]Department of Science Education, Howard Hughes Medical Institute, Chevy Chase, MD 20815; [h]Biological Imaging Section, Research Technologies Branch, National Institute of Allergy and Infectious Diseases, NIH, Bethesda, MD 20892; [i]Department of Applications Science, BioLegend, San Diego, CA 92121; and [j]Surgical Oncology Program, Metastasis Biology Section, Center for Cancer Research, National Cancer Institute, NIH, Bethesda, MD 20892

Contributed by Ronald N. Germain, November 11, 2020 (sent for review September 3, 2020; reviewed by Marc K. Jenkins and Lai Guan Ng)

The diverse composition of mammalian tissues poses challenges for understanding the cell–cell interactions required for organ homeostasis and how spatial relationships are perturbed during disease. Existing methods such as single-cell genomics, lacking a spatial context, and traditional immunofluorescence, capturing only two to six molecular features, cannot resolve these issues. Imaging technologies have been developed to address these problems, but each possesses limitations that constrain widespread use. Here we report a method that overcomes major impediments to highly multiplex tissue imaging. "Iterative bleaching extends multiplexity" (IBEX) uses an iterative staining and chemical bleaching method to enable high-resolution imaging of >65 parameters in the same tissue section without physical degradation. IBEX can be employed with various types of conventional microscopes and permits use of both commercially available and user-generated antibodies in an "open" system to allow easy adjustment of staining panels based on ongoing marker discovery efforts. We show how IBEX can also be used with amplified staining methods for imaging strongly fixed tissues with limited epitope retention and with oligonucleotide-based staining, allowing potential cross-referencing between flow cytometry, cellular indexing of transcriptomes and epitopes by sequencing, and IBEX analysis of the same tissue. To facilitate data processing, we provide an open-source platform for automated registration of iterative images. IBEX thus represents a technology that can be rapidly integrated into most current laboratory workflows to achieve high-content imaging to reveal the complex cellular landscape of diverse organs and tissues.

high-dimensional imaging | tissue immunity | quantitative microscopy | immune system | immunofluorescence

Mammalian tissues are composed of a wide variety of cell types, presenting a major challenge to understanding the cell–cell interactions required for homeostasis as well as the compositional changes associated with disease. To address this complexity, several multiplexed imaging methods utilizing conventional microscopes and commercially available antibodies have been described to overcome the target detection limitations of conventional immunohistochemistry (IHC) or immunofluorescence (IF) imaging (1–8). The majority of these methods generate high-dimensional datasets through an iterative, multistep process (i.e., a cycle) that includes 1) immunolabeling with antibodies, 2) image acquisition, and 3) fluorophore inactivation or antibody/chromogen removal. While these methods are capable of generating high-dimensional datasets, they are greatly limited by the number of markers visualized per cycle or length of time required for each cycle, or they involve special fluid-handling platforms not generally available to most laboratories (1). Commercial systems based on the codetection by indexing method (9) have facilitated the acquisition of multiplex imaging data by providing a fully automated instrument for cyclic imaging. Despite this advancement, the proprietary nature of this method imposes constraints on the reagents available for use as well as the number of markers to be imaged for each round. Furthermore, cyclic imaging methods that employ a small number of markers per cycle (i.e., fewer than three) may result in tissue loss due to the stress of repeated fluid exchanges. To this end, imaging techniques such as multiplexed ion beam imaging (10) and imaging mass cytometry (11) enable the capture of multiparameter data without cyclic imaging. However, both of these methods require specialized instrumentation and consumables, with the latter often again limited in breadth to choices made by the supplier, not the investigator. This constrains their capacity for broadly analyzing human or

IMMUNOLOGY AND INFLAMMATION

Significance

Single-cell flow cytometry and genomic methods are rapidly increasing our knowledge of the diversity of cell types in metazoan tissues. However, suitably robust methods for placing these cells in a spatial context that reveals how their localization and putative interactions contribute to tissue physiology and pathology are still lacking. Here we provide a readily accessible pipeline (IBEX) for highly multiplex immunofluorescent imaging that enables a fine-grained analysis of cells in their tissue context. Additionally, we describe extensions of the IBEX workflow to handle hard-to-image tissue preparations and a method to facilitate direct integration of the imaging data with flow cytometry and sequencing technologies.

Author contributions: A.J.R., E.K., E.S., C.J.C., A.G., R.S., and R.N.G. designed research; A.J.R., E.K., B.L., E.S., C.J.C., A.G., N.T., R.S., Z.R.Y., R.T.B., and J.K. performed research; J.C., J.D., and J.M.H. contributed new reagents/analytic tools; A.J.R., E.K., B.L., E.S., C.J.C., A.G., N.T., R.S., Z.R.Y., R.T.B., J.K., and R.N.G. analyzed data; A.J.R. and R.N.G. wrote the paper; and L.Y. designed schematics for figures.

Reviewers: M.K.J., University of Minnesota Medical School; and L.G.N., Singapore Immunology Network.

Competing interest statement: J.C. is an employee of BioLegend, which manufactures and sells TotalSeq-A antibodies that are used in one of the workflows described in this paper.

See online for related content such as Commentaries.

[1]A.J.R. and E.K. contributed equally to this work.

[2]To whom correspondence may be addressed. Email: andrea.radtke@nih.gov or rgermain@niaid.nih.gov.

This article contains supporting information online at https://www.pnas.org/lookup/suppl/doi:10.1073/pnas.2018488117/-/DCSupplemental.

First published December 21, 2020.

experimental animal tissues with respect to lists of validated antibodies, the ability to work across various established protocols for tissue processing, and the capacity for real-time changes to the epitope target list based on data emerging from high-content methods such as single-cell RNA sequencing (scRNA-seq).

To address the increasing need for high-content analysis of tissues for projects such as the Human Cell Atlas and others, the field requires a fully open and extensible method for multiplex imaging. Our laboratory has extensively characterized murine and human immune responses using quantitative multiparameter imaging of fixed frozen samples (12–18). Importantly, this method of tissue fixation preserves tissue architecture and cellular morphology, is archivable and compatible with large-volume imaging (19), and, in its optimal form, eliminates technical challenges posed by formalin-fixed, paraffin-embedded (FFPE) samples. Leveraging this experience and our original single-cycle histocytometry method for multiplex data acquisition (12), we have now developed "iterative bleaching extends multiplexity" (IBEX). This imaging technique reduces the time per cycle, uses a high number of antibodies per cycle, employs widely available reagents and instruments, provides open-source software for image alignment, and minimizes physical damage to the tissue during multiple imaging cycles. Beyond the basic IBEX workflow, we have developed extensions to achieve multiparameter imaging of heavily fixed tissues with limited retention of target epitopes and have incorporated commercially available oligonucleotide-conjugated antibodies to enable direct cross-comparisons to flow cytometry and scRNA-seq data obtained by the cellular indexing of transcriptomes and epitopes by sequencing (CITE-seq) method (20). In addition to describing the specifics of the IBEX procedure, we provide multiple examples of the use of IBEX to analyze both immune and parenchymal cells in a diverse array of mouse and human tissues to illustrate the general applicability of the technique. The IBEX method described here can be rapidly integrated into current laboratory workflows to obtain high-dimensional imaging datasets from a wide range of animal and human tissues.

Results

IBEX Builds and Improves upon Existing Iterative Imaging Techniques. Iterative imaging methods typically use either fluorophore bleaching or antibody/chromogen removal to obtain multiparameter datasets (1–8). Due to the harsh and variable conditions required to remove chromogens and antibodies with diverse target affinities, we pursued a strategy based on fluorophore bleaching. To achieve an efficient means to increase the number of markers visualized on a single section, we sought an inactivation method that could bleach a wide range of fluorophores in minutes without epitope loss or tissue destruction. While H_2O_2 in alkaline solution has been reported to inactivate Cy3- and Cy5-conjugated antibodies in human FFPE samples (3), we observed significant tissue loss using this formulation over multiple cycles with fixed frozen samples (*SI Appendix*, Fig. S1*A*). Adams et al. demonstrated the initial feasibility of using borohydride derivates to bleach fluorophores; however, their fluorophore quenching method required 2 h per cycle and comprised only three distinct imaging channels (6), making direct application for highly multiplex imaging impractical. To expand upon this method, we tested antibodies directly conjugated to fluorophores with excitation and emission spectra spanning from 405 nm to 750 nm. We consistently found that the following fluorophores were inactivated within 15 min of exposure to 1 mg/mL of lithium borohydride ($LiBH_4$): Pacific blue, Alexa Fluor (AF) 488, fluorescein isothiocyanate (FITC), AF532, phycoerythrin (PE), AF555, eFluor (eF) 570, AF647, eF660, and AF700. Brilliant Violet conjugates BV421 and BV510 bleached within 15 min of exposure to 1 mg/mL of $LiBH_4$ in the presence of light. In contrast, AF594, eF615, and the nuclear markers JOJO-1 and Hoechst required more than 120 min for significant loss of fluorescence signal (*SI Appendix*, Table S1), permitting these probes to be used as fiducials for alignment of images emerging from iterative cycles.

To prevent tissue destruction over multiple cycles, we evaluated several different tissue adhesives and found that chrome gelatin alum securely adhered tissues to glass coverslips and slides, permitting more than 15 cycles to be performed with no appreciable loss to the tissue (*SI Appendix*, Fig. S1 *B* and *C*). We next reduced the antibody labeling time from 6 to 12 h to 30 to 45 min by designing programs for a nonheating microwave that facilitates rapid antibody penetration into the section. Finally, although IBEX was designed to simply bleach the fluorophores, it was important to assess whether $LiBH_4$ treatment physically removes antibodies from the tissue, as this would have direct bearing on both the design and order of imaging panels. To examine this issue, mouse lymph node (LN) sections were immunolabeled with various primary antibodies, imaged, treated with $LiBH_4$, and then incubated with a secondary antibody that would react with the primary antibody if it was still present on the tissue. For most of the antibody isotypes tested, we found almost identical staining patterns with the primary and secondary antibodies, indicating that $LiBH_4$ acts primarily by fluorophore bleaching without stripping the fluorescently conjugated antibodies themselves (*SI Appendix*, Fig. S2).

The resulting method, IBEX, reduces the fluorophore inactivation and antibody labeling steps to less than 1 h (Fig. 1*A*). We first tested IBEX in practical use by examining the image quality that could be obtained from a three-cycle analysis of mouse LNs (Fig. 1*B*), a tissue with which we had extensive experience using multiparameter, single-cycle staining and image collection. This initial test used six to eight markers per cycle and showed that all fluorophores, except for AF594 and JOJO-1, bleached rapidly in the presence of $LiBH_4$ treatment with or without light, with no appreciable signal present after 10 min (Fig. 1 *C* and *D*). These findings show that the IBEX pipeline performs as designed and allows for the rapid capture of high-quality, multiplexed imaging data over multiple cycles without tissue loss.

A SimpleITK Image Registration Pipeline. The IBEX method yields a series of images that are collected separately. To properly process these data and correctly assign markers to individual cells, it is essential that all of the images be aligned at high resolution. While various registration algorithms have been reported (21, 22), we sought a method that could align large datasets, was flexible in terms of the repeated markers (fiducials) utilized, and provided both a qualitative and quantitative metric for registration. For these reasons, we developed a workflow using SimpleITK, a simplified open-source interface to the Insight Toolkit (ITK) that is compatible with multiple programming languages (23, 24). The SimpleITK workflow is an image intensity-based form of image alignment that relies on a repeated marker channel (fiducial) for registration. Due to the resistance of AF594, JOJO-1, and Hoechst to bleaching, we utilized markers in these fluorophores as fiducials. For a multicycle IBEX experiment, a "fixed" image *z*-stack was selected, and all other "moving" images were resampled to this image. A cross-correlation matrix was generated on the repeated marker channels to provide a quantitative means for assessing the quality of image registration (Fig. 2*A*). To test the fidelity of this method, a three-cycle IBEX experiment was performed on mouse spleen sections labeled with the nuclear marker JOJO-1 and membrane label CD4 AF594. For these experiments, JOJO-1 was selected as the fiducial used for image registration; however, CD4 (also repeated in these experiments) showed pixel-to-pixel alignment as reflected in the images (Fig. 2*B*). Importantly, this platform can readily scale to handle large datasets (>260 GB) comprised of 20 cycles of imaging (*SI Appendix*, Fig. S1 *B*–*D*). The SimpleITK registration workflow thus provides the needed cell–cell registration across *x*–*y*–*z* dimensions obtained via iterative imaging cycles using IBEX.

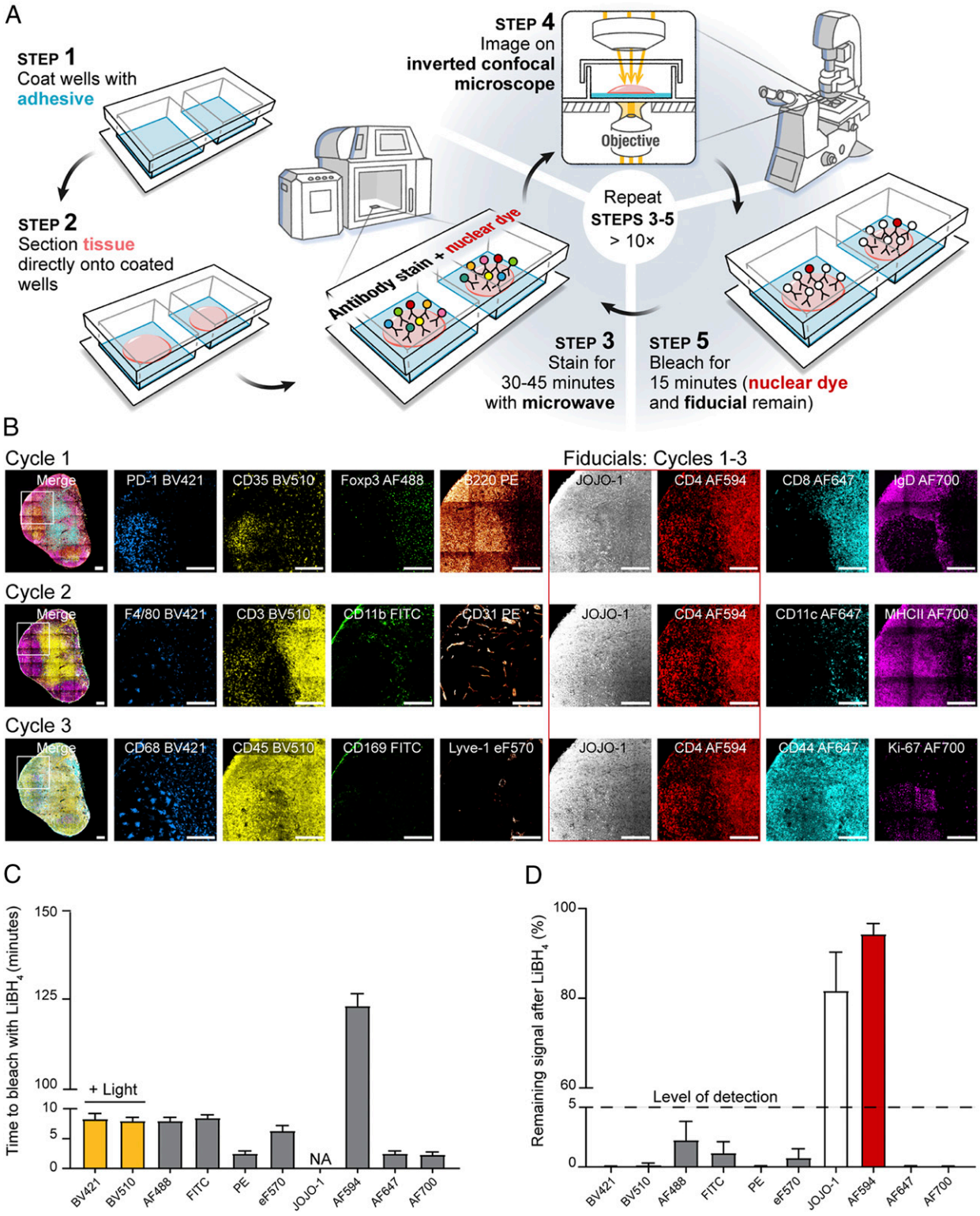

Fig. 1. IBEX is a high-dimensional, iterative imaging technique. (*A*) Schematic depicting IBEX protocol. (*B*) Mice were immunized subcutaneously (s.c.) with 25 μL of SRBCs on day 0 and 7. On day 14, pLN tissue sections were labeled with three separate imaging panels. (Scale bar: 150 μm.) Light refers to bleaching with $LiBH_4$ while the sample was illuminated with a metal halide lamp and DAPI filter. (*C*) Time required to bleach respective fluorophores using $LiBH_4$. NA, no appreciable loss of signal over multiple hours of $LiBH_4$ exposure. (*D*) Percentage of fluorophore signal remaining after 15 min of $LiBH_4$ treatment. Data are pooled from two similar experiments and presented as mean ± SEM.

IBEX Is a Versatile Imaging Method. One obstacle to the wide adoption of existing multiplex imaging methods is the need for specialized instruments or custom imaging chambers, a luxury not afforded to all laboratories. In contrast, IBEX is easily adaptable to diverse microscope systems and has no restrictions on the substrate (e.g., slide, coverslip) used for imaging

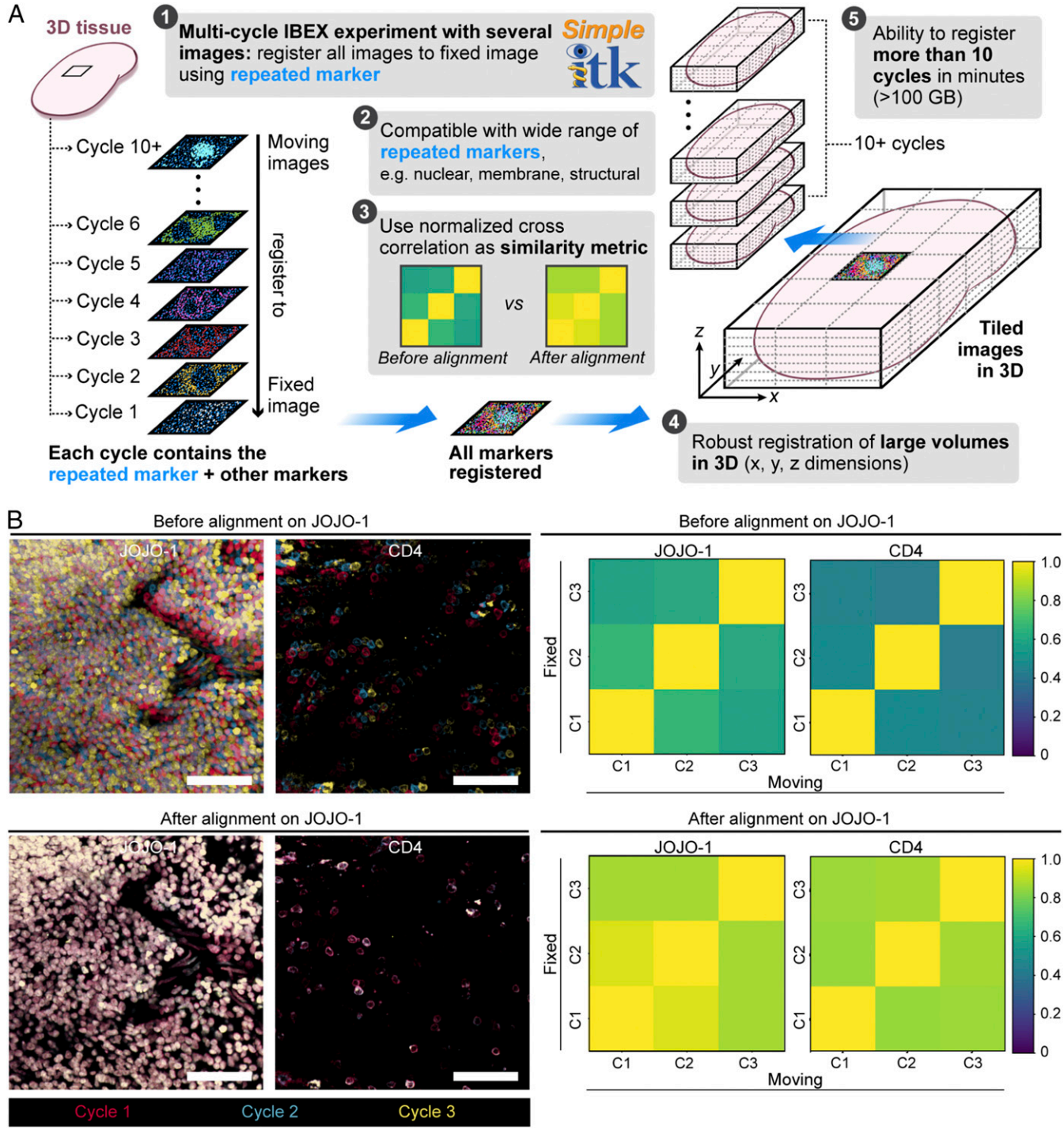

Fig. 2. Image alignment with SimpleITK image registration pipeline. (*A*) Workflow for SimpleITK image registration pipeline. (*B*) Confocal images showing JOJO-1 and CD4 from three consecutive IBEX cycles before and after alignment using the nuclear marker JOJO-1 as a fiducial across all three cycles ("*C*," *Right*). CD4 was also repeated and shows cell–cell registration after JOJO-1 alignment. (Scale bar: 50 μm.) Cross-correlation similarity matrices before and after alignment with JOJO-1 for JOJO-1 and CD4 channels. All experiments are representative of at least two similar experiments.

(*SI Appendix*, Fig. S3*A*). As a proof of concept, immunized mouse LN sections adhered to slides were visualized using an upright confocal microscope ($n = 4$ cycles, $n = 6$ markers per cycle) or an inverted fluorescence microscope ($n = 4$ cycles, $n = 4$ markers per cycle; *SI Appendix*, Fig. S3 *B* and *C*). These results demonstrate the compatibility of IBEX with a wide range of imaging systems; however, it is worth noting that the microscope system (confocal versus widefield) and configuration (light source, detectors, filter cubes) will dictate the image acquisition time, number of markers per cycle, and sample type that can be effectively imaged (5- vs. 30-μm tissue thickness).

In the case of animal studies, it is also very useful to be able to integrate antibody staining with imaging of fluorescent marker proteins expressed by engineered cells transferred into animals or expressed in situ. We therefore next investigated whether the IBEX method could be used to image tissues from animals

expressing fluorescent proteins (25). To this end, high-dimensional imaging was performed on thymic tissues from transgenic animals expressing the following fluorescent proteins (FPs): cyan FP (CFP), green FP (GFP), yellow FP (YFP), and red FP (RFP) (26). No appreciable loss in signal was observed after 10 IBEX cycles for any of the FPs examined (*SI Appendix*, Fig. S4 *A* and *B*). The photostable FPs were used as fiducials for a four-cycle IBEX experiment that incorporated the bleachable fluorophores AF647 and AF700, yielding a dataset that provided information on clonality (CFP, GFP, YFP, RFP) of T cells (CD4, CD8, Foxp3) and myeloid cells (CD11c, MHC II) in the thymus (*SI Appendix*, Fig. S4*C*).

To determine how IBEX performs using sections from a variety of tissues, we performed experiments using three to five cycles of IBEX with sections from murine spleen, thymus, lung, small intestine, and liver (Fig. 3 *A* and *B* and Movies S1–S5 and *SI Appendix*, Table S2). It is important to note that the cycle and marker numbers described here are provided as a proof of concept and do not reflect technical limitations of the method. The antibody panels were designed to capture the major cellular populations and structures present in each organ, and fluorophores were chosen to avoid native tissue autofluorescence. Organ-specific fiducials were selected based on expression throughout the tissue, e.g., EpCAM to mark the epithelium of the small intestine and laminin for the liver sinusoids. Collectively, these data confirm the ability to use IBEX to obtain high-quality, multiplexed imaging datasets from a wide range of tissues.

IBEX Enables Highly Multiplex, Quantitative Imaging. The design principles of IBEX were chosen to enable a very high number of parameters to be attained in the analysis of an individual tissue sample. To determine how extensively the multiplexing capacity of IBEX can be pushed, we first performed 10-cycle, 41-parameter IBEX experiments on LNs obtained from naïve and sheep red blood cell (SRBC)-immunized mice (Fig. 4*A* and *SI Appendix*, Table S2 and Movie S6). While epitope loss has been described for other iterative imaging techniques (5), we minimized this problem by increasing the number of markers per cycle and grouping markers present on the same cell in the same cycle. We observed qualitatively similar staining patterns when antibody panels were applied on individual sections alone (serial) versus on the same section iteratively (IBEX; *SI Appendix*, Fig. S5*A* and Movie S7). Therefore, quantitative differences observed between the two methods likely reflect biological differences resulting from variations in the magnitude of the immune response in individual LNs and not technical differences associated with epitope loss or steric hindrance (*SI Appendix*, Fig. S5*B* and Movie S7).

To assess the quality of data generated by the IBEX method, we employed the open-source, computational histology topography cytometry analysis toolbox (histoCAT) to quantify differences in LN organization resulting from immunization (27). Individual cells were segmented based on membrane and nuclear labels with Ilastik (28) and CellProfiler (29) and then analyzed using the histoCAT graphical user interface (*SI Appendix*, Fig. S6*A*). The unsupervised clustering algorithm Phenograph (30) identified 29 phenotype clusters shared across the naïve and immunized LNs that could be visualized using the data dimensionality reduction method t-SNE (31) in histoCAT (Fig. 4*B*). As a testament to the fidelity of cell–cell alignment, phenotype clusters were often characterized by the expression of several different markers present in distinct imaging cycles (*SI Appendix*, Fig. S6 *B* and *C*). The abundance of these cell phenotypes varied from naïve and immunized LNs (*SI Appendix*, Fig. S6*D*) and could be manually annotated based on marker expression to reveal an increase in plasma cells (PCs; cluster 10) and germinal center (GC) B cells (cluster 6) in immunized LNs (Fig. 4*C*). As histoCAT relies on nuclear and membrane-based cell segmentation, it suffers from limitations frequently encountered with this approach: miscalling of phenotypes due to spatial overlap

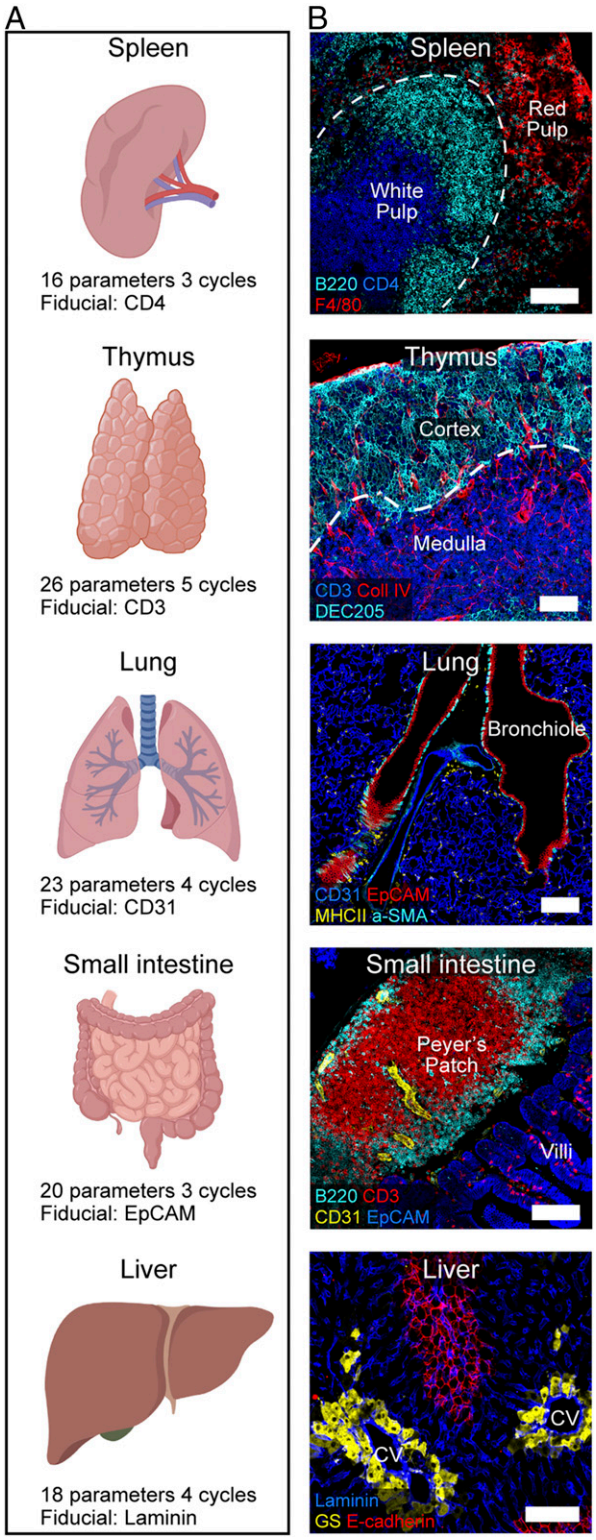

Fig. 3. IBEX in multiple murine organs. (*A*) IBEX experimental parameters. (*B*) Confocal images from IBEX experiments in various mouse organs. Liver: central vein (CV) and glutamine synthetase (GS). (Scale bar: 100 μm.) Movies S1–S5 show additional details.

and improper segmentation of nonlymphocyte populations (32). The former is evident in the identification of the B cell-specific transcription factor pax5 (33) on $CD3^+CD4^+PD\text{-}1^+Bcl6^+$

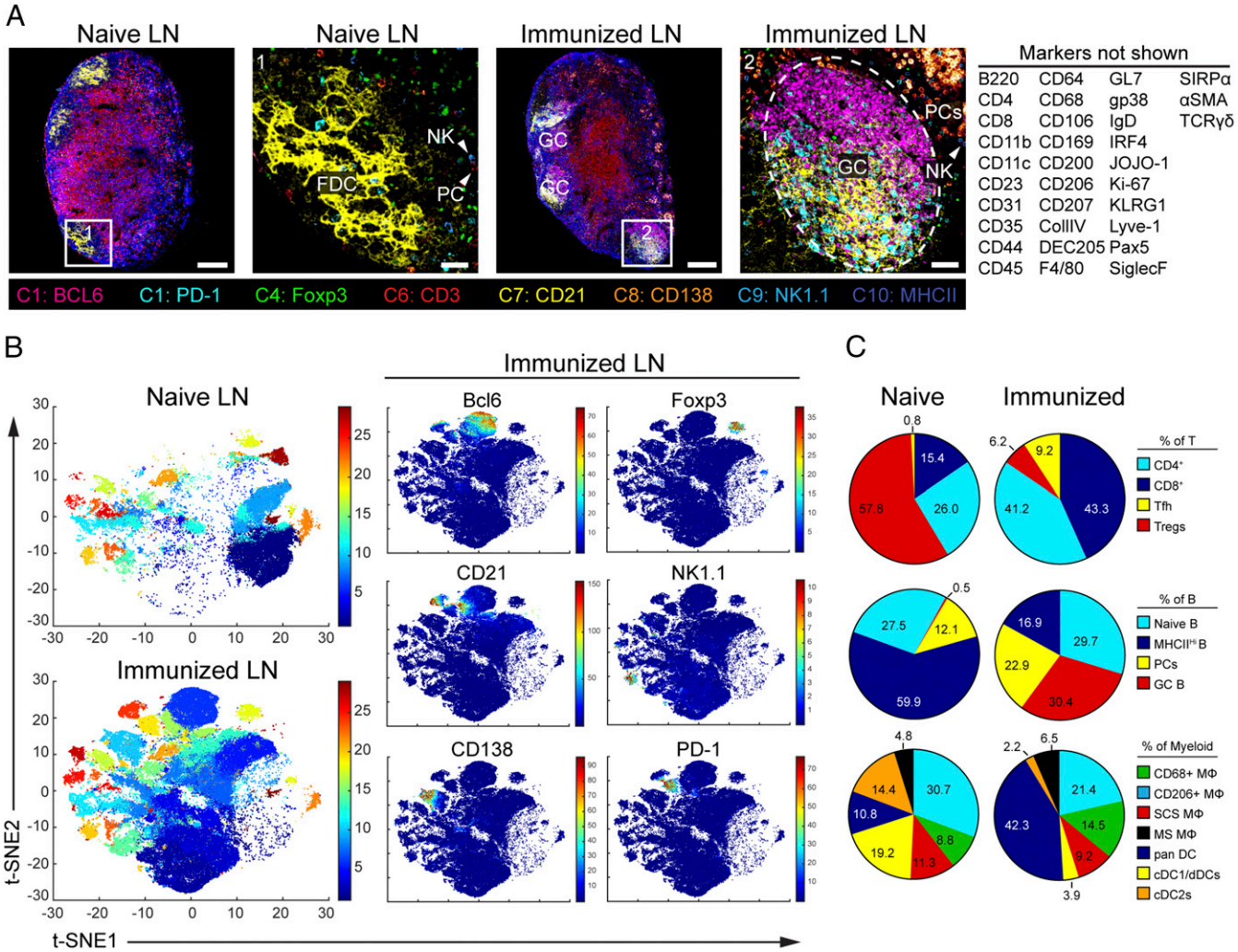

Fig. 4. Visualization and quantification of LN populations using IBEX and histoCAT following immune perturbation. (*A*) Confocal images of pLNs from naïve and SRBC-immunized mice from 10-cycle ("C" at bottom), 41-parameter IBEX experiments. NK, natural killer; FDC, follicular DC. (Scale bars: left to right, 100 μm, 25 μm, 100 μm, and 50 μm.) (*B*) t-SNE plots from naïve and immunized LNs identified by Phenograph clustering using segmented cells in histoCAT (naïve, n = 32,091; immune, n = 80,355). Color reflects the cluster ID number (from 1 to 29). Single plots show separation of representative markers into discrete clusters, with color map showing relative expression levels based on Z score-normalized marker intensity values. (*C*) Phenograph clusters identified by histoCAT were phenotyped based on marker expression and expressed as a proportion of lineage. MΦ, macrophage; SCS, subcapsular sinus; MSM, medullary sinus; dDC, dermal DC. Data are from one experiment and representative of two similar experiments (*SI Appendix*, Fig. S6 and Movie S6).

T follicular helper (Tfh) cells (cluster 19), an artifact due to the close proximity of these cells within the GC (*SI Appendix*, Fig. S6*C*). Nevertheless, the results presented here demonstrate that IBEX-generated images are compatible with established methods for analyzing high-dimensional imaging data.

IBEX Scales to Capture Ultra High-Content Data from Large Areas of Human Tissues. In addition to capturing the cellular landscape of a diverse range of murine tissues, the IBEX method scales to enable high-content imaging of human tissues. To this end, we present an application of the IBEX method to visualize tumor–immune interactions in a human pancreatic LN with metastatic lesions as shown by $CD138^+EpCAM^+$ cells in the LN capsule and sinuses (Fig. 5*A* and *SI Appendix*, Table S3). Interestingly, cancer cells were segregated from lymphocytes by extensive collagen remodeling and recruitment of myeloid cells expressing the secreted protein acidic and rich in cysteine (SPARC), a matricellular glycoprotein involved in extracellular matrix deposition and implicated in metastasis (34). To move to an even deeper analysis of a much larger sample, we used a total of 66 antibodies for the analysis of a >3-mm^2 human mesenteric LN section. Using this approach, we were able to deeply phenotype a wide range of immune cells while observing no tissue degradation over 20 cycles (Fig. 5*B* and Movie S8 and *SI Appendix*, Table S3). Additionally, we observed subcellular resolution for PC-specific markers (membrane, CD138; nuclear, IRF4; cytoplasmic, IgA1, IgA2) present in distinct cycles with no epitope loss, as evidenced by our ability to label the immune marker CD45 with two different antibody clones present in cycles 9 and 19 (Movie S8). The utility of this method is further exemplified by our ability to characterize the complex stroma of the LN, shown to contain nine distinct clusters in scRNA-seq experiments from mouse LNs (35), using a wide range of antibodies visualized in situ: α-SMA, CD21, CD23, CD34, CD35, CD49a, CXCL12, CXCL13, desmin, fibronectin, and vimentin. These data highlight the capacity of IBEX to identify a large number of distinct cell types in clinically relevant samples, while also placing these components in a spatial setting missed by methods employing dissociated single cells.

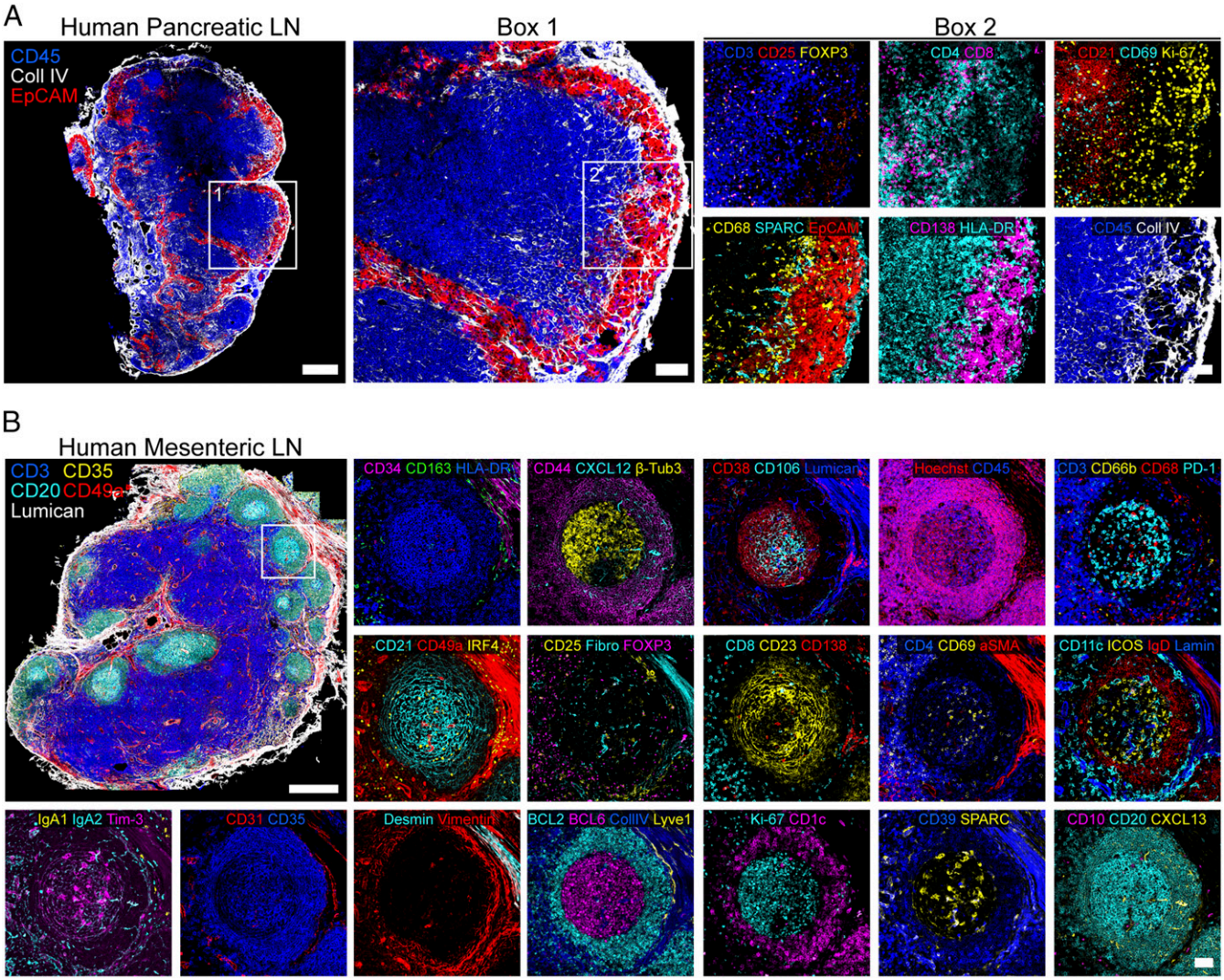

Fig. 5. IBEX scales to capture ultra high-content imaging in human tissues. (*A*) Confocal images from a pancreatic LN with metastatic lesions from a patient with colorectal cancer (4 cycles, 17 parameters). (Scale bars: *Left*, 500 μm; box 1, 100 μm; box 2, 50 μm). (*B*) Confocal images from human mesenteric LN (20 cycles, 66 parameters). (Scale bars: 500 μm or 50 μm.) Fibro, fibronectin; Lamin, laminin. Movie S8 shows additional details.

Extensions of IBEX Workflow. Given the inherent versatility of the IBEX method, we sought to extend our workflow to develop two unique protocols, one that enables detection of low abundance epitopes and another that permits iterative imaging with oligonucleotide-conjugated antibodies corresponding to those used in scRNA-seq experiments. Opal IHC, a method of signal amplification that employs incubation with an unconjugated primary, followed by a horseradish peroxidase (HRP)-conjugated secondary, and deposition of Opal fluorophore in the tissue, is an attractive method for detection of very low levels of specific proteins (36). We first tested this method by staining for endogenous levels of the chemokine CXCL9 in the liver sinusoids of mice (*SI Appendix*, Fig. S7*A*), which showed a signal not readily detected with direct or indirect staining methods. Further, because Opal IHC is well described for the imaging of fixed (i.e., FFPE) human tissues (37, 38), we next evaluated whether this method could be expanded upon to achieve multiparameter imaging of tissues from high containment facilities. Due to the extreme fixation conditions required to inactivate select agents such as the Ebola virus (10% formalin for 8 d), the majority of stainable epitopes are lost in these tissues (39, 40). To overcome this significant technical limitation, we developed the Opal-plex method that is based on the IBEX pipeline. Opal-plex extends the usual fluorophore limitations of Opal by combining multiplex Opal IHC with cycles of IBEX-based bleaching to eliminate signal from $LiBH_4$-sensitive dyes (Opal 570, 650, and 690) while utilizing the $LiBH_4$-resistant dye (Opal 540) as a fiducial (Fig. 6*A* and *SI Appendix*, Fig. S7*B*). Using this approach, we achieved single-cell resolution of 10 unique markers in heavily fixed mouse LNs (Fig. 6*B* and Movie S9).

We next evaluated whether oligonucleotide-conjugated antibodies, including those used for CITE-seq, are compatible with our IBEX workflow. While immunolabeling with oligonucleotide-conjugated antibodies is well established (9), the use of a large number of commercially available TotalSeq-A antibodies with publicly available oligo-tag sequences, the employment of nonproprietary buffers for hybridization and dehybridization, and the use of a wide spectrum of fluorophore-labeled complementary oligonucleotides provides a truly open-source system with many advantages. In particular, the imaging method described here applies the same antibodies used for scRNA-seq, permitting direct comparison between imaging and CITE-seq datasets while providing a much-needed spatial context for the cell populations identified. Using this approach, we were able to achieve high-quality tissue staining with

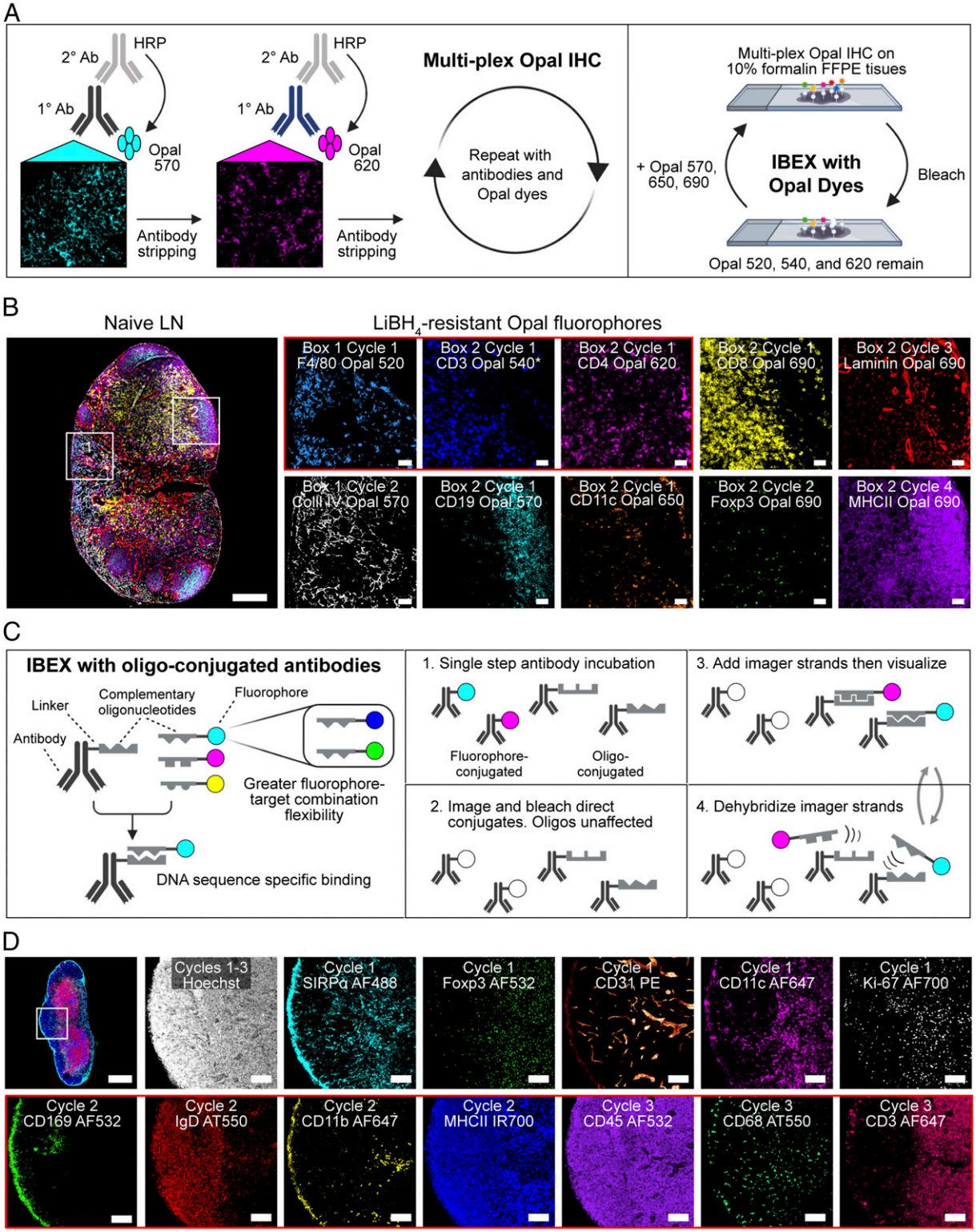

Fig. 6. Incorporation of Opal fluorophores and oligo-conjugated antibodies into IBEX workflow. (*A*) Opal-plex imaging method. (*B*) Representative images from a 10-parameter, 4-cycle Opal-plex experiment performed on 5-μm FFPE tissue sections from heavily fixed mouse pLNs. CD3 Opal 540 was present throughout cycles 1 through 4 and served as a fiducial (asterisk). (Scale bars: 50 μm; leftmost panel, 200 μm.) (*C*) IBEX with oligo-conjugated antibodies method. (*D*) Confocal images from a 13-parameter, 3-cycle IBEX experiment performed on 20-μm tissue sections from an immunized inguinal mouse LN. Cycle 1: fluorophore-conjugated antibodies. Cycles 2 and 3: oligo-conjugated antibodies, Atto550 (AT550). (Scale bars: 50 μm; *Top Left*, 400 μm.) Data are representative of three similar experiments (*SI Appendix*, Fig. S7 and Movie S9).

five unique fluorophores (*SI Appendix*, Fig. S7*C*). This method can be directly integrated into our IBEX protocol, alongside fluorophore-conjugated antibodies when CITE-seq antibodies to desired targets do not exist, as $LiBH_4$ bleaching leaves oligonucleotide binding intact (Fig. 6 *C* and *D*). Importantly, the quality of staining achieved with oligonucleotide-conjugated antibodies, even after multiple cycles of $LiBH_4$ bleaching, is comparable to conventional IF, as quantitative differences, e.g., higher expression of MHCII on dendritic cells (DCs) versus B cells, can still be observed (Fig. 6*D* and *SI Appendix*, Fig. S7*D* and Movie S9). In summary, this protocol improves upon existing high-dimensional DNA-based imaging techniques by offering full flexibility in antibody–fluorophore pairing, integrating commercially produced CITE-seq reagents, reducing antibody labeling to one step, and extending the number of fluorophores per cycle.

Discussion

Multiplex imaging of tissues is increasingly important for studies of tumor–immune interactions, for discovery efforts such as the Human Cell Atlas, for better understanding of pathological events in infected or physically damaged tissues, and for placing data from isolated cells in the context of in situ tissue organization. IBEX is a broadly applicable technique that utilizes conventional microscopes and commercially available antibodies to obtain these essential high-dimensional imaging data. IBEX improves upon existing iterative methods by addressing many of the limitations inherent to these techniques. First, we have significantly reduced the fluorophore inactivation step and antibody labeling time from >16 h to <1 h using a rapid chemical bleaching agent and antibody labeling employing a commercial nonheating microwave. Second, our selection of the bleaching agent $LiBH_4$ provides an efficient means to bleach over 15 unique fluorophores while preserving select fluorophores to serve as repeated markers for registration. Importantly, $LiBH_4$ treatment does not cause tissue or epitope loss, as evidenced by our ability to obtain highly multiplexed data over several cycles in a wide range of tissues with a very large number of antibodies. Third, and integral to the preservation of tissue integrity through multiple fluid handling cycles, was the use of the tissue adhesive chrome gelatin alum. Importantly, this adhesive adheres delicate tissues to the slide or coverslip surface while maintaining key anatomical features. Finally, the SimpleITK workflow described here represents a significant advancement for the registration of images obtained via cyclic IF methods. In addition to offering flexibility in terms of the repeated markers (membrane, nuclear, structural) used, it provides alignment of markers present on the same cell but not utilized as the fiducial. This is a critical standard for all high-dimensional imaging methods because multiple markers are often required to phenotype a particular cell type, and staining for the relevant epitopes may occur in different imaging cycles.

In addition to developing an efficient method for highly multiplexed imaging, the IBEX workflow, unlike commercial all-in-one systems (9–11), offers flexibility in terms of cellular markers, antibody–fluorophore combinations, and microscope configurations employed. Because the chemistry of bleaching depends on the fluorophore and not the antibody to which it is conjugated, once the bleaching conditions are defined, staining panels can be designed using specific combinations of fluorophores without regard for the target epitopes of the antibodies employed, providing the user with extreme versatility in experimental design. To this end, we report the validation of more than 200 commercially available antibodies conjugated to fluorophores with excitation and emission spectra ranging from 405 nm to 750 nm. Furthermore, we demonstrate that commercially available oligonucleotide-conjugated antibodies can be seamlessly integrated into our IBEX workflow, representing an application of TotalSeq-A antibodies for in situ IHC. Given that the barcode sequences for TotalSeq-A antibodies are disclosed, and a wide range of fluorophore-conjugated oligos are readily available, fluorophore and antibody pairing can be fully customized to match microscope configuration, epitope abundance, and unique tissue characteristics. Taken together, the oligonucleotide-staining method described here provides a completely open method to achieve highly multiplexed IF imaging using the same antibodies employed for flow cytometry and/or CITE-seq, enabling effective cross-referencing of datasets derived from these complementary technologies.

As a proof of concept, we have used the IBEX workflow to examine such issues as the visualization of difficult-to-extract myeloid populations in various tissues, changes in immune cell composition following immune perturbation, and detection of low abundance epitopes. For the first application, we were able to visualize tissue-resident macrophages that are difficult to characterize using other methods such as flow cytometry because of their limited recovery upon enzymatic tissue digestion (12). Using the panels of antibodies outlined here, we were able to deeply phenotype medullary ($CD169^+F4/80^+CD11b^+Lyve\text{-}1^{+/-}$) and subcapsular sinus ($CD169^+F4/80^-CD11b^+$) macrophages in the LNs (41), as well as alveolar ($SiglecF^+CD11b^-CD11c^+$) and interstitial ($CD11b^+CD11c^+MHCII^+$) macrophages of the lung (42). Additionally, we show that the IBEX method can be scaled to capture ultra high-content imaging in human tissues. The ability to survey large areas of human tissue is critically important, as all possible information needs to be extracted to provide maximally useful clinical and research data.

Beyond simple visualization of diverse cell types, we have shown compatibility between IBEX-generated data and downstream single-cell, spatially resolved analysis using the open-source method histoCAT. From the 10-cycle IBEX experiments described above, the histoCAT workflow identified 29 phenotype clusters characterized by the expression of several different markers present in distinct imaging cycles. Importantly, this approach identified well described changes following immunization such as an increase in Tfh cells and GC B cells (43). Finally, incorporation of multiplex Opal IHC into our IBEX workflow facilitated the detection of low abundance epitopes present in conventionally fixed tissues while aiding in the detection of epitopes lost under extreme fixation conditions. The latter represents a significant achievement because few studies have visualized the immunopathology induced by select agents and, to date, the largest number of parameters examined in a single section has been limited to three (44). The ability to use IBEX in its native format and with the Opal-plex variation is especially valuable in the context of the current COVID-19 pandemic. Preliminary data show that these methods work well with highly fixed postmortem samples from such patients.

In summary, IBEX constitutes a versatile technique for obtaining high-content imaging data using conventional microscopes and commercially available antibodies. In addition to providing a valuable resource for studying tissue-based immunity in animal models of disease, ongoing studies have shown the value of the IBEX method to provide a spatially defined assessment of complex cell phenotypes from diverse organs including lung, kidney, heart, and lymphoid tissues from surgical specimens as well as postmortem samples from human COVID-19 patients. We believe that the open nature of the reagents that can be utilized, and the variety of instruments suitable for implementation of IBEX, make it an attractive method for many laboratories seeking to obtain a deeper understanding of cell composition and spatial organization in tissues of interest.

Materials and Methods

Detailed descriptions of animals, immunization and tissue preparations, reagents, imaging protocols with Opal fluorophores and oligonucleotide-conjugated

antibodies, microscopy configurations, and image acquisition and analysis details are reported in *SI Appendix, Supplemental Methods*.

Mouse and Human Tissues. Murine organs and human LNs (1 cm^3 or smaller in size) were fixed with BD CytoFix/CytoPerm (BD Biosciences) diluted in phosphate-buffered saline (PBS) solution (1:4) for 2 d at 4 °C. Following fixation, all tissues were washed briefly (5 min per wash) in PBS and incubated in 30% sucrose for 2 d at 4 °C before embedding in OCT compound (Tissue-Tek). All mice were maintained in specific pathogen-free conditions at an Association for Assessment and Accreditation of Laboratory Animal Care accredited animal facility at the National Institute of Allergy and Infectious Diseases (NIAID). All procedures were approved by the NIAID Animal Care and Use Committee (NIH). Deidentified LN samples were obtained from patients undergoing elective risk-reducing gastrectomies or colon resections for colon adenocarcinoma at the National Cancer Institute (NCI) based on an institutional review board-approved tissue collection protocol (13C-0076).

IBEX Using Inverted Confocal Microscope. Sections (20 to 30 μm) were cut on a CM1950 cryostat (Leica) and adhered to two-well Chambered Coverglasses (Lab-Tek) coated with 15 μL of chrome alum gelatin (Newcomer Supply) per well. Frozen sections were permeabilized, blocked, and stained in PBS containing 0.3% Triton X-100 (Sigma-Aldrich), 1% BSA (Sigma-Aldrich), and 1% mouse or human Fc block (BD Biosciences). For conventional IF, sections were first blocked for 1 to 2 h at room temperature and then stained for 12 h at 4 °C in a humidity chamber. For microwave-assisted IF, we utilized the PELCO BioWave Pro-36500-230 microwave equipped with a PELCO SteadyTemp Pro-50062 thermoelectric recirculating chiller (Ted Pella). A 2–1–2–1–2–1–2–1–2 program was used for immunolabeling, where "2" denotes 2 min at 100 W and "1" denotes 1 min at 0 W. The above program was executed once for blocking and secondary antibody labeling and twice for primary antibody labeling. A complete list of antibodies and tissue-specific panels is provided in *SI Appendix*, Tables S1–S5. Cell nuclei were visualized with JOJO-1 (Thermo Fisher Scientific) or Hoechst (Biotium), and sections were mounted using Fluoromount G (Southern Biotech). Mounting media was thoroughly removed by washing with PBS after image acquisition and before chemical bleaching of fluorophores. Samples were treated with 1 mg/mL of $LiBH_4$ (STREM Chemicals) prepared in diH_2O for 15 min to bleach all fluorophores except JOJO-1, Hoechst, eF615, and Alexa Fluor 594. To bleach antibodies conjugated to Brilliant Violet 421 (BV421) and Brilliant Violet 510 (BV510) dyes, tissue sections were illuminated using the metal halide lamp with the DAPI filter of the Leica TCS SP8 X inverted confocal microscope. The efficiency of fluorophore bleaching was assessed in real time by viewing the $LiBH_4$-incubated samples on the microscope. Following efficient bleaching, the $LiBH_4$ solution was removed, and samples were washed in three exchanges of PBS, restained with the next panel, and mounted with Fluoromount G. Fluorophore inactivation with H_2O_2 was conducted as described previously (5), with tissue sections being treated for 1 h at room temperature with 4.5% H_2O_2 (Sigma) prepared in an alkaline solution. Tissue sections were imaged as described in *SI Appendix, Supplemental Methods*.

Image Alignment and Registration. The alignment of all IBEX panels to a common coordinate system was performed using SimpleITK (23, 24). To facilitate registration, we utilized a common channel present in all panels. As the images may differ by a significant translational motion, we use a Fourier domain-based initialization approach (45) that accommodates this motion. In addition, we utilized SimpleITK's multiscale registration framework with four levels, reducing the resolution by a factor of two per level. Directly using the original voxel sizes, on the order of 10^{-3} mm, in the gradient descent optimizer computations leads to numerical instability. We therefore normalized the voxel dimensions during optimization while preserving anisotropy. The final, optimal transformations are then used to resample all channels from each panel to the common coordinate system. The software repository for SITK_IBEX is provided at https://github.com/niaid/sitk-ibex.

Extensions of IBEX Protocol. Integrating IBEX with Opal dyes or oligonucleotide-conjugated antibodies was performed as detailed in *SI Appendix, Supplemental Methods*. For multiplex Opal IHC, the following steps were repeated to achieve six-plex imaging using the Opal 520, 540, 570, 620, 650, and 690 fluorophores: primary antibody incubation, incubation with HRP-conjugated secondary, labeling with Opal dye, and antibody stripping. After representative images were captured, coverslips were removed and tissue sections were treated with 1 mg/mL of $LiBH_4$ prepared in diH_2O for 30 min to bleach the Opal 570, 650, and 690 dyes. Cycles of multiplex Opal IHC and IBEX were repeated to achieve the desired number of markers. For integration of oligonucleotide-conjugated antibodies into the IBEX workflow, TotalSeq-A antibodies were incubated with fluorophore-conjugated antibodies, which were imaged first before $LiBH_4$ bleaching. Oligonucleotides are preserved, and complementary fluorophore-conjugated oligonucleotides are used to reveal immunostaining, then either dehybridized or bleached again in situ across multiple cycles.

Data Availability. All study data are included in the article and supporting information.

ACKNOWLEDGMENTS. This research was supported by the Intramural Research Program of the NIH, NIAID, and NCI. This research was also partially supported by a Research Collaboration Agreement (RCA) between NIAID and BioLegend (RCA 2020-0333). C.J.C. is supported as a UK–US Fulbright Scholar. We thank Dr. Jagan Muppidi for assistance with SRBC immunization and tissue harvest. Figures were created with Biorender.com.

1. W. Schubert, Topological proteomics, toponomics, MELK-technology. *Adv. Biochem. Eng. Biotechnol.* **83**, 189–209 (2003).
2. W. Schubert *et al*., Analyzing proteome topology and function by automated multidimensional fluorescence microscopy. *Nat. Biotechnol.* **24**, 1270–1278 (2006).
3. M. J. Gerdes *et al*., Highly multiplexed single-cell analysis of formalin-fixed, paraffin-embedded cancer tissue. *Proc. Natl. Acad. Sci. U.S.A.* **110**, 11982–11987 (2013).
4. J. R. Lin, M. Fallahi-Sichani, P. K. Sorger, Highly multiplexed imaging of single cells using a high-throughput cyclic immunofluorescence method. *Nat. Commun.* **6**, 8390 (2015).
5. J. R. Lin *et al*., Highly multiplexed immunofluorescence imaging of human tissues and tumors using t-CyCIF and conventional optical microscopes. *eLife* **7**, e31657 (2018).
6. D. L. Adams, R. K. Alpaugh, S. Tsai, C. M. Tang, S. Stefansson, Multi-Phenotypic subtyping of circulating tumor cells using sequential fluorescent quenching and restaining. *Sci. Rep.* **6**, 33488 (2016).
7. T. Tsujikawa *et al*., Quantitative multiplex immunohistochemistry reveals myeloid-inflamed tumor-immune complexity associated with poor prognosis. *Cell Rep.* **19**, 203–217 (2017).
8. G. Gut, M. D. Herrmann, L. Pelkmans, Multiplexed protein maps link subcellular organization to cellular states. *Science* **361**, 6401 (2018).
9. Y. Goltsev *et al*., Deep profiling of mouse splenic architecture with CODEX multiplexed imaging. *Cell* **174**, 968–981.e15 (2018).
10. M. Angelo *et al*., Multiplexed ion beam imaging of human breast tumors. *Nat. Med.* **20**, 436–442 (2014).
11. C. Giesen *et al*., Highly multiplexed imaging of tumor tissues with subcellular resolution by mass cytometry. *Nat. Methods* **11**, 417–422 (2014).
12. M. Y. Gerner, W. Kastenmuller, I. Ifrim, J. Kabat, R. N. Germain, Histo-cytometry: A method for highly multiplex quantitative tissue imaging analysis applied to dendritic cell subset microanatomy in lymph nodes. *Immunity* **37**, 364–376 (2012).
13. W. Kastenmüller, P. Torabi-Parizi, N. Subramanian, T. Lämmermann, R. N. Germain, A spatially-organized multicellular innate immune response in lymph nodes limits systemic pathogen spread. *Cell* **150**, 1235–1248 (2012).
14. K. Mao *et al*., Innate and adaptive lymphocytes sequentially shape the gut microbiota and lipid metabolism. *Nature* **554**, 255–259 (2018).
15. A.P. Baptista *et al*., The chemoattractant receptor Ebi2 drives intranodal naive CD4(+) T cell peripheralization to promote effective adaptive immunity. *Immunity* **50**, 1188–1201.e6 (2019).
16. S. Uderhardt, A.J. Martins, J.S. Tsang, T. Lammermann, R.N. Germain, Resident macrophages cloak tissue microlesions to prevent neutrophil-driven inflammatory damage. *Cell* **177**, 541–555.e17 (2019).
17. C. Petrovas *et al*., Follicular CD8 T cells accumulate in HIV infection and can kill infected cells in vitro via bispecific antibodies. *Sci. Transl. Med.* **9**, 373 (2017).
18. I. Sayin *et al*., Spatial distribution and function of T follicular regulatory cells in human lymph nodes. *J. Exp. Med.* **215**, 1531–1542 (2018).
19. W. Li, R. N. Germain, M. Y. Gerner, Multiplex, quantitative cellular analysis in large tissue volumes with clearing-enhanced 3D microscopy (C_e3D). *Proc. Natl. Acad. Sci. U.S.A.* **114**, E7321–E7330 (2017).
20. M. Stoeckius *et al*., Simultaneous epitope and transcriptome measurement in single cells. *Nat. Methods* **14**, 865–868 (2017).
21. P. Thévenaz, U. E. Ruttimann, M. Unser, A pyramid approach to subpixel registration based on intensity. *IEEE Trans. Image Process.* **7**, 27–41 (1998).
22. M. Guizar-Sicairos, S. T. Thurman, J. R. Fienup, Efficient subpixel image registration algorithms. *Opt. Lett.* **33**, 156–158 (2008).
23. B. C. Lowekamp, D. T. Chen, L. Ibáñez, D. Blezek, The design of SimpleITK. *Front. Neuroinform.* **7**, 45 (2013).
24. Z. Yaniv, B. C. Lowekamp, H. J. Johnson, R. Beare, SimpleITK image-analysis notebooks: A collaborative environment for education and reproducible research. *J. Digit. Imaging* **31**, 290–303 (2018).
25. S. Li *et al*., Overview of the reporter genes and reporter mouse models. *Animal Model. Exp. Med.* **1**, 29–35 (2018).
26. H. J. Snippert *et al*., Intestinal crypt homeostasis results from neutral competition between symmetrically dividing Lgr5 stem cells. *Cell* **143**, 134–144 (2010).
27. D. Schapiro *et al*., histoCAT: Analysis of cell phenotypes and interactions in multiplex image cytometry data. *Nat. Methods* **14**, 873–876 (2017).

28. S. Berg *et al*., ilastik: Interactive machine learning for (bio)image analysis. *Nat. Methods* **16**, 1226–1232 (2019).
29. A. E. Carpenter *et al*., CellProfiler: Image analysis software for identifying and quantifying cell phenotypes. *Genome Biol.* **7**, R100 (2006).
30. J. H. Levine *et al*., Data-driven phenotypic dissection of AML reveals progenitor-like cells that correlate with prognosis. *Cell* **162**, 184–197 (2015).
31. A. D. Amir *et al*., viSNE enables visualization of high dimensional single-cell data and reveals phenotypic heterogeneity of leukemia. *Nat. Biotechnol.* **31**, 545–552 (2013).
32. B. Bodenmiller, Multiplexed epitope-based tissue imaging for discovery and healthcare applications. *Cell Syst.* **2**, 225–238 (2016).
33. C. Cobaleda, A. Schebesta, A. Delogu, M. Busslinger, Pax5: The guardian of B cell identity and function. *Nat. Immunol.* **8**, 463–470 (2007).
34. S. Sangaletti *et al*., Macrophage-derived SPARC bridges tumor cell-extracellular matrix interactions toward metastasis. *Cancer Res.* **68**, 9050–9059 (2008).
35. L.B. Rodda *et al*., Single-Cell RNA Sequencing of lymph node stromal cells reveals niche-associated heterogeneity. *Immunity* **48**, 1014–1028.e16 (2018).
36. E. C. Stack, C. Wang, K. A. Roman, C. C. Hoyt, Multiplexed immunohistochemistry, imaging, and quantitation: A review, with an assessment of tyramide signal amplification, multispectral imaging and multiplex analysis. *Methods* **70**, 46–58 (2014).
37. E.R. Parra *et al*., Validation of multiplex immunofluorescence panels using multispectral microscopy for immune-profiling of formalin-fixed and paraffin-embedded human tumor tissues. *Sci. Rep.* **7**, 13380 (2017).
38. M. A. J. Gorris *et al*., Eight-color multiplex immunohistochemistry for simultaneous detection of multiple immune checkpoint molecules within the tumor microenvironment. *J. Immunol.* **200**, 347–354 (2018).
39. R. W. Dapson, Macromolecular changes caused by formalin fixation and antigen retrieval. *Biotech. Histochem.* **82**, 133–140 (2007).
40. J. D. Webster, M. A. Miller, D. Dusold, J. Ramos-Vara, Effects of prolonged formalin fixation on diagnostic immunohistochemistry in domestic animals. *J. Histochem. Cytochem.* **57**, 753–761 (2009).
41. E. E. Gray, J. G. Cyster, Lymph node macrophages. *J. Innate Immun.* **4**, 424–436 (2012).
42. A. V. Misharin, L. Morales-Nebreda, G. M. Mutlu, G. R. Budinger, H. Perlman, Flow cytometric analysis of macrophages and dendritic cell subsets in the mouse lung. *Am. J. Respir. Cell Mol. Biol.* **49**, 503–510 (2013).
43. G. D. Victora, M. C. Nussenzweig, Germinal centers. *Annu. Rev. Immunol.* **30**, 429–457 (2012).
44. A. Greenberg *et al*., Quantification of viral and host biomarkers in the liver of rhesus macaques: A longitudinal study of Zaire ebolavirus strain kikwit (EBOV/Kik). *Am. J. Pathol.* **190**, 1449–1460 (2020).
45. D. Padfield, Masked object registration in the Fourier domain. *IEEE Trans. Image Process.* **21**, 2706–2718 (2012).

Supplementary Information for

IBEX – A versatile multi-plex optical imaging approach for deep phenotyping and spatial analysis of cells in complex tissues

Andrea J. Radtke[1,11,*], Evelyn Kandov[2,3,11], Bradley Lowekamp[4], Emily Speranza[2,5], Colin J. Chu[2], Anita Gola[2,6], Nishant Thakur[2], Rochelle Shih[2,6], Li Yao[7], Ziv Rafael Yaniv[4], Rebecca T. Beuschel[1], Juraj Kabat[8], Joshua Croteau[9], Jeremy Davis[10], Jonathan M. Hernandez[10], and Ronald N. Germain[1,2,*]

[1]Center for Advanced Tissue Imaging, Laboratory of Immune System Biology, NIAID, NIH, Bethesda, MD, USA

[2]Lymphocyte Biology Section, Laboratory of Immune System Biology, NIAID, NIH, Bethesda, MD, USA

[3]Vanderbilt University School of Medicine, Nashville, TN, USA

[4]Bioinformatics and Computational Bioscience Branch, NIAID, NIH, Bethesda, MD, USA

[5]Innate Immunity and Pathogenesis Section, Laboratory of Virology, NIAID, NIH, Hamilton, MT, USA

[6]The Rockefeller University, New York, NY, USA

[7]Howard Hughes Medical Institute, Chevy Chase, MD, USA

[8]Biological Imaging Section, Research Technologies Branch, NIAID, NIH, Bethesda, MD, USA

[9]BioLegend, Inc., San Diego, CA, USA

[10]Surgical Oncology Program, Metastasis Biology Section, Center for Cancer Research, National Cancer Institute, NIH

[11]Co-first authors

[*]Co-corresponding authors: Andrea Radtke (andrea.radtke@nih.gov); Ronald Germain, (rgermain@niaid.nih.gov)

This PDF includes:

Supplemental Methods

Figures S1-S7 and Legends

Tables S1-S5

Movies S1-S9 Legends

SI References

Supplemental Methods

Animals, immunizations, and tissue preparations

5-12 week old naïve C57BL/6 and *Cxcl9*$^{-/-}$ mice were purchased from Jackson Laboratories (Bar Harbor, ME) and maintained at a facility at the NIH. Fluorescent Confetti animals were generated by crossing B6.129P2-Gt(ROSA)26Sortm1(CAG-Brainbow2.1)Cle/J × B6.Cg-Tg(UBC-cre/ERT2)1Ejb/2J and LysM-tdTomato mice were generated by crossing LysM-Cre x B6.Cg-Gt(ROSA)26Sortm14(CAG-tdTomato)Hze/J (Jackson Laboratory). Fluorescent Confetti animals heterozygous for both transgenes were injected intraperitoneally (i.p.) with tamoxifen 100 µg per gram of body weight in peanut oil (Sigma-Aldrich) on day 0 and day 2 and tissues were collected on day 4 for processing. To evaluate changes in the immune cell composition and LN architecture following immunization, sheep red blood cells (SRBCs, Colorado Serum Company) were prepared by resuspending 3 mL of SRBCs in 10 mL of Hanks' Balanced Salt Solution (HBSS, Sigma-Aldrich). Mice were injected subcutaneously (s.c.) with SRBCs in a volume of 25-50 µl per site on day 0 and day 4 with organs harvested on day 11. Unless stated otherwise, all tissues were treated similarly and embedded as whole organs. Prior to fixation, murine livers and lungs were perfused with PBS in order to remove blood. The ileal portion of the small intestine was excised and prepared using the Swiss roll technique (1). Livers were collected from LysM-tdTomato mice and processed as described previously (2). Lungs were inflated with 10 ml of fixative via a tracheal cannula before harvest (3). Lungs were then tethered to a small weight and fixed overnight in BD CytoFix/CytoPerm (BD Biosciences) diluted in PBS (1:4). Following fixation, all tissues were washed briefly (5 minutes per wash) in PBS and incubated in 30% sucrose for 2 days before embedding in OCT compound (Tissue-Tek).

Additional considerations for IBEX method

For optimal results, it is important to be aware of the expiration date of the chrome gelatin alum and to follow these steps for coating chambers and glass slides: 1) spread the adhesive evenly over the imaging substrate, 2) dry 1 hour at 60° C, 3) section tissue onto coated chamber or glass slide, 4) dry for 1 hour at 37° C, and 5) work with freshly prepared samples (don't store at -20° C). In order to achieve efficient bleaching, always use 1 mg/ml solutions of $LiBH_4$ within 4 hours of preparation and wait until large bubbles form before adding to tissue (usually 10 minutes after dissolving in diH_2O). Be careful as $LiBH_4$ can react violently with water. To avoid flames, always work with small amounts (<10 mg) of $LiBH_4$. Store $LiBH_4$ with desiccant and use a new vial of $LiBH_4$ after 4 weeks of use. As noted in the "IBEX using inverted confocal microscope" section of the Methods section, Brilliant Violet 421 (BV421) and Brilliant Violet 510 (BV510) dyes require $LiBH_4$ bleaching in the presence of light (metal halide lamp with the DAPI filter). To ensure efficient

bleaching of BV421 and BV510 conjugates, we assess bleaching in real time by viewing the $LiBH_4$-incubated samples under the microscope, bleaching a field of view (1-2 minutes), and moving to an adjacent field of view (1-2 minutes). This process is repeated until the entire region of interest is bleached. Of note, the time required for this process is dependent on the imaging area and objective used for bleaching with larger areas requiring longer overall bleaching times. As an example, a tissue section from a mouse LN (1-2 mm) can be readily bleached in 15 minutes using this approach. Another consideration is that all images be oriented identically in the Z stack (same begin and end) for proper alignment with SimpleITK. For gross observation and visualization, we found that IBEX-generated images could be aligned using Imaris 9.5.0 (Bitplane) by "adding images" and manually aligning images with the reference manager. Alternatively, the image alignment feature under the image processing menu was used to provide a rough assessment of image registration before submitting IBEX-generated images to the SimpleITK workflow.

Ensuring optimal imaging quality: Antibody validation and controls

Selection of antibodies that bind their targets with great specificity while yielding reproducible immunolabeling across different samples is critical for all imaging methods. Wherever possible, we utilize highly cited antibodies previously validated for immunofluorescence of fixed frozen tissues. Upon identifying suitable antibody candidates for our imaging workflow, we note the location (membrane, cytoplasm, nucleus) and tissue distribution of the marker of interest. Additionally, we procure positive and negative control tissues based on the described expression of a particular marker. Finally, we pair the new antibody with previously validated markers that co-stain the same cell type. For example, the SPARC antibody (R&D AF941) is reported to label macrophages, fibroblasts, and endothelial cells within human tissues. To validate this antibody, we evaluate the spatial distribution of the anti-SPARC antibody in human LNs co-stained with CD3 (negative) and CD11c and CD31 (positive controls). Prior to all iterative imaging, antibodies are tested for their sensitivity to $LiBH_4$ by pretreating tissue sections with $LiBH_4$ for 15 minutes. To evaluate whether epitopes are sensitive to $LiBH_4$, staining patterns for individual antibodies are compared between serial sections with or without $LiBH_4$ pre-treatment. As an additional control, individual panels are acquired on serial sections in parallel with iterative rounds of imaging. The spatial distribution patterns are then compared between the serially and iteratively acquired images for each antibody to ensure there is no epitope loss or steric hindrance with cyclic imaging. Finally, antibody concentrations vary greatly depending on the tissue, fixation conditions, and imaging system employed. For these reasons, we strongly recommend careful titration of all antibodies prior to IBEX imaging.

IBEX imaging conditions for inverted confocal microscope

Representative sections from different tissues were acquired using an inverted Leica TCS SP8 X confocal microscope equipped with a 40X objective (NA 1.3), 4 HyD and 1 PMT detectors, a white light laser that produces a continuous spectral output between 470 and 670 nm as well as 405, 685, and 730 nm lasers. Panels consisted of antibodies conjugated to the following fluorophores and dyes: Hoechst, BV421, BV510, AF488, AF532, JOJO-1, PE, eF570, AF555, AF594, AF647, eF660, and AF700. All images were captured at an 8-bit depth, with a line average of 3, and 1024x1024 format with the following pixel dimensions: x (0.284 μm), y (0.284 μm), and z (1-1.25 μm). Images were tiled and merged using the LAS X Navigator software (LAS X 3.5.5.19976). To ensure proper alignment over distinct imaging cycles, careful attention was paid to the quality of image stitching achieved with the Leica software and z-stacks were set by manual inspection of notable features such as unusually shaped nuclei throughout the tissue volume. These unusual features were matched across the z-stack and over multiple cycles of IBEX.

Adoption of IBEX to additional imaging systems

For adoption of the IBEX protocol to an upright Leica TCS SP8 X confocal microscope, 20-30 µm sections were adhered to Super Frost Plus Gold slides (Electron Microscopy Services) coated with 30 µl of chrome alum gelatin. The IBEX protocol was executed as described above with the following exceptions: slides were mounted with a No. 1.5 coverslip (VWR) and antibody panels were designed without BV421 and BV510 conjugated antibodies. These conjugates were omitted because they require the tissue to be immersed in $LiBH_4$ while illuminated with the metal halide lamp, an impossibility for samples mounted on slides. Following image acquisition, coverslipped slides were immersed in PBS until the coverslip floated off. Non-coverslipped slides were incubated with $LiBH_4$ for 15 minutes, washed extensively in PBS, immunolabeled with the next round of antibodies, mounted with Fluoromount G, and coverslipped. Image acquisition parameters and system configurations were identical to the details listed for the inverted Leica TCS SP8 X confocal microscope with the exception of the 685 nm laser. For adoption of the IBEX protocol to an inverted fluorescent microscope, 5-10 µm sections were adhered to Super Frost Plus Gold slides coated with chrome alum gelatin. Slides were mounted with a coverslip and antibody panels were designed with the following fluorophores and dyes: Hoechst (Biotium), AF488, PE, and AF647. Representative sections were acquired using a Keyence BZ-X800 microscope equipped with a 40X objective, metal halide lamp, and DAPI, GFP, TRITC, and Cy5 filter sets. All images were captured using the auto-exposure settings for each channel at standard resolution yielding an 8-bit image. Haze reduction was applied post-acquisition to improve image quality.

Image analysis and quantification

Fluorophore emission was collected on separate detectors with sequential laser excitation of compatible fluorophores (3-4 per sequential) used to minimize spectral spillover. The Channel Dye Separation module within the LAS X 3.5.5.19976 (Leica) was then used to correct for any residual spillover. Threshold identification, voxel gating, surface creation, and masking were performed as previously described (4, 5). For publication quality images, gaussian filters, brightness/contrast adjustments, and channel masks were applied uniformly to all images. Unless stated otherwise, images are presented as maximum intensity projections (MIP) of tiled z-stacks. Quantification of cell surfaces was based on images with unadjusted gamma values. To calculate the amount of signal remaining after $LiBH_4$ bleaching (Figs. 1D and S7B), the Color Pixel Counter plugin developed by Ben Pichette for FIJI was used (6). The Structural SSIMilarity (SSIM) index, a method for measuring the similarity between 2 images, was used to assess whether $LiBH_4$ treatment removed primary antibodies from the tissues (7) (Fig. S2). The surface creation module of Imaris 9.5.0 (Bitplane) was used to segment cells based on the nuclear marker Hoechst (Figs. S1C or S5B) or CFP+, GFP+, YFP+, or RFP+ expression (Fig. S4B). For consistency, segmentation conditions were applied as a batch using identical parameters. Segmented cells were randomly colored and manually inspected to assess the quality of segmentation based on Hoechst or FP staining. For Fig. S5B, segmentation on Hoechst+ cells provided accurate identification of round, regular shaped, lymphocytes but, as expected, struggled with morphologically complex stromal and structural cell segmentation. Nevertheless, this approach provided a relative quantification for the number of surfaces positive for each individual marker. Importantly, these qualitative measures were in agreement with the amount of signal present by visual inspection. Surfaces were scored positive for a given marker based on absolute intensity values generated in Imaris and these values were applied uniformly to serial and IBEX-generated images to quantify marker-positive surfaces (Fig. S5B).

histoCAT analysis of IBEX-generated images

Using the workflow described previously (8), IBEX-generated images were segmented using Ilastik (Version 1.3.3) (9) and CellProfiler (Version 3.1.9) (10). Briefly, B220, CD3, and CD45 (most of the immune cells) markers were merged into a single membrane and JOJO-1 was used as a nuclear marker. Membrane and nuclear Images were loaded into Ilastik for supervised training of pixel segmentation. The trained Ilastik model classified image pixels into 3 classes (membrane, nuclear, and background) and generated probability maps for CellProfiler for cellular objects segmentation. CellProfiller-generated object/mask images were exported as TIFF files for downstream analysis. To quantify marker expression, individual marker images, along with masks, were loaded into histoCAT and Phenograph clustering with default parameters was performed. Phenograph consistently identified 29 different clusters/phenotypes (Fig. 4B). Hierarchical clustering and heatmap (Fig. S6B) were generated from the Phenograph output using the Seaborn

Python package. The high-dimensional single-cell data was projected onto 2 dimensions using the t-SNE module in histoCAT for visualization purposes shown in Fig. 4B. Cellular populations identified in Fig. 4C were manually phenotyped based on the cellular markers expressed within each Phenograph cluster and summarized in the heat map found in Fig. S6B: $CD4^+$ T (cluster 3), $CD8^+$ T (cluster 2), Tfh (cluster 19), Tregs (cluster 18), naïve B (cluster 5), $MHCII^{Hi}$ B (cluster 13), PCs (cluster 10), GC B (cluster 6), $CD68^+$ macrophages (cluster 15), $CD206^+$ macrophages (cluster 11), SCS macrophages (cluster 17), MS macrophages (cluster 25), pan DC (cluster 4), cDC1/dDCs (cluster 22), and cDC2s (cluster 26). A median of ratios method (11) was performed for the cell count normalization (Fig. S6D). All histoCAT analysis was done on an iMAC, (Retina 5K, 27-inch, 2017, 4.2Ghz i7, 64G RAM) with macOS Mojave operating system.

Multi-plex Opal IHC on heavily fixed tissues

pLNs were collected from naïve mice and fixed at 4° C for 8 days in 10% neutral-buffered formalin (Cancer Diagnostics). Following fixation, samples were washed in PBS to remove formalin and embedded in paraffin blocks. 5 µm sections were cut from paraffin blocks, mounted on slides, and left at 37° C for 16 hours to dry. Slides were incubated at 60° C for 45 minutes, dewaxed using a standard protocol of 10 minutes in xylene (2 times), and rehydrated with graded concentrations of ethanol and water (100% ethanol for 10 minutes, 95% ethanol for 10 minutes, 70% ethanol for 5 minutes). Following dewaxing, slides were first rinsed in water and tissues were fixed to the slides by placing in 10% formalin for 15 minutes, rinsed in water, and then placed in TBST (1X TBS + 0.5% Tween20 (Thermo)) to prevent drying out. Antigen retrieval was performed using the AR6 buffer from the Opal Multi-plex kit (Akoya Biosciences) using a conventional microwave at 100% power for 45 seconds followed by 10% power for 15 minutes. To perform multi-plex Opal IHC, tissue sections were first blocked in Opal antibody diluent/blocking buffer (Akoya Biosciences) for 10 minutes. Next, unconjugated primary antibodies were added to the tissue for 12-16 hours at 4° C, 4 hours at room temperature, or 30 minutes using the PELCO BioWave Pro 36500-230 microwave described under 'IBEX using inverted confocal microscope' section of the Material and Methods. After primary antibody incubation, samples were washed with TBST and an Opal anti-rabbit HRP-conjugated secondary antibody was added at a dilution of 1:5 for 10 minutes at room temperature or with a species matched HRP-conjugated secondary antibody for 1 hour at room temperature. Samples were washed several (5-6) times with TBST and Opal dyes (diluted 1:100 in 1X amplification buffer (Akoya Biosciences)) were added to the sample and incubated for 10 minutes at room temperature. Following this last step, samples were washed with TBST and antigen retrieval/antibody stripping was performed using the AR6 buffer and conventional microwave treatment described above. This series of steps—primary antibody incubation, incubation with HRP-conjugated secondary, labeling with Opal dye, antibody stripping—was repeated for the following Opal fluorophores to achieve 6-plex imaging: Opal 520, 540, 570, 620,

650, and 690. Slides were mounted and imaged with an upright Leica TCS SP8 X confocal microscope as described above. After representative images were captured, coverslips were removed and tissue sections were treated with 1 mg/mL of $LiBH_4$ prepared in diH_2O for 30 minutes to bleach the Opal 570, 650, and 690 dyes. Cycles of multi-plex Opal IHC and IBEX were repeated to achieve the desired number of markers. Individual images were aligned and processed as described above. A complete list of antibodies and reagents can be found in Table S4.

Chemokine staining for endogenous CXCL9

Livers were collected from naïve WT and *Cxcl9*$^{-/-}$ animals, perfused with 1% PFA through the portal vein, and fixed at 4° C for 12-16 hours in BD CytoFix/CytoPerm diluted 1:4 in PBS. Samples were incubated in sucrose for 24 hours at 4° C and frozen in OCT. To visualize endogenous CXCL9 levels, 20 µm sections were rehydrated in PBS, incubated in 0.1% H_2O_2 for 30 minutes to quench endogenous peroxidase, and incubated with unconjugated (CXCL9) and fluorescently-conjugated primary antibodies. Tissue sections were washed to remove unbound antibodies, fixed with 10% formalin to cross-link the bound antibodies to the tissue, washed with TBST, and an Opal anti-rabbit HRP-conjugated secondary antibody was added at a dilution of 1:5 for 10 minutes at room temperature. Following secondary antibody incubation, samples were washed in TBST and the Opal 650 dye (diluted 1:100 in 1X amplification buffer) was added for 5 minutes. Slides were washed, mounted in Fluoromount G, and imaged as described above. A complete list of antibodies and reagents can be found in Table S4.

Incorporation of TotalSeqA™ antibodies into IBEX workflow

LNs from C57BL/6 mice were harvested and processed as described above. Integrating published methods, slides containing 30 µm sections were blocked for 30 minutes at room temperature in Buffer A (PBS supplemented with 5% donkey serum (Jackson Immunoresearch), 200 µg/ml sheared salmon sperm (Thermo), 0.2% Triton X-100 (Sigma) and 5 µg/ml Fc-block (Thermo)). Immunolabeling was conducted using Buffer A with the addition of 5 mM EDTA and 0.02% Dextran sulfate, TotalSeqA™ antibodies (5 µg/ml), and fluorophore-conjugated antibodies at the indicated concentrations (Table S1) (12). All primary antibody incubations were performed using the PELCO BioWave Pro 36500-230 microwave as described in the “IBEX using inverted confocal microscope’ section of the Materials and Methods. Following antibody incubation, slides were washed using PBS with 0.1% Triton X-100 and post-fixed with 5 mM of BS(PEG)5 (Thermo) for 10 minutes before quenching with 100 mM Ammonium Chloride (Sigma). After washing with PBS, Fluoromount G was applied and fluorescently-conjugated antibodies were imaged in the first cycle. Mounting medium was removed by washing with PBS before bleaching with $LiBH_4$ for 15 minutes. For *in situ* visualization of TotalSeqA™ antibodies, oligonucleotides were designed

complementary to the TotalSeqA™ barcode. These complementary oligonucleotides were synthesized by Integrated DNA Technologies (IDT) and 5'-end conjugated with indicated fluorophores before HPLC purification (Table S5). Direct labeling of TotalSeqA™ antibodies with complementary fluorescent oligonucleotides was achieved by adding 1 µM concentrations of imager oligonucleotides in PBS with 0.1% Triton X-100 and incubating for 30 minutes at room temperature. Tissue sections were washed with 0.5X PBS and 0.1% Triton X-100, mounted, and imaged (Cycle 2 of IBEX). After removal of Fluoromount G, oligonucleotides were dehybridized for 15 minutes by incubation with a 0.1X PBS solution containing 30% Formamide. Following 5-6 exchanges of PBS, the next set of oligonucleotides (Cycle 3) was applied as before.

Figures S1-S7 and Legends

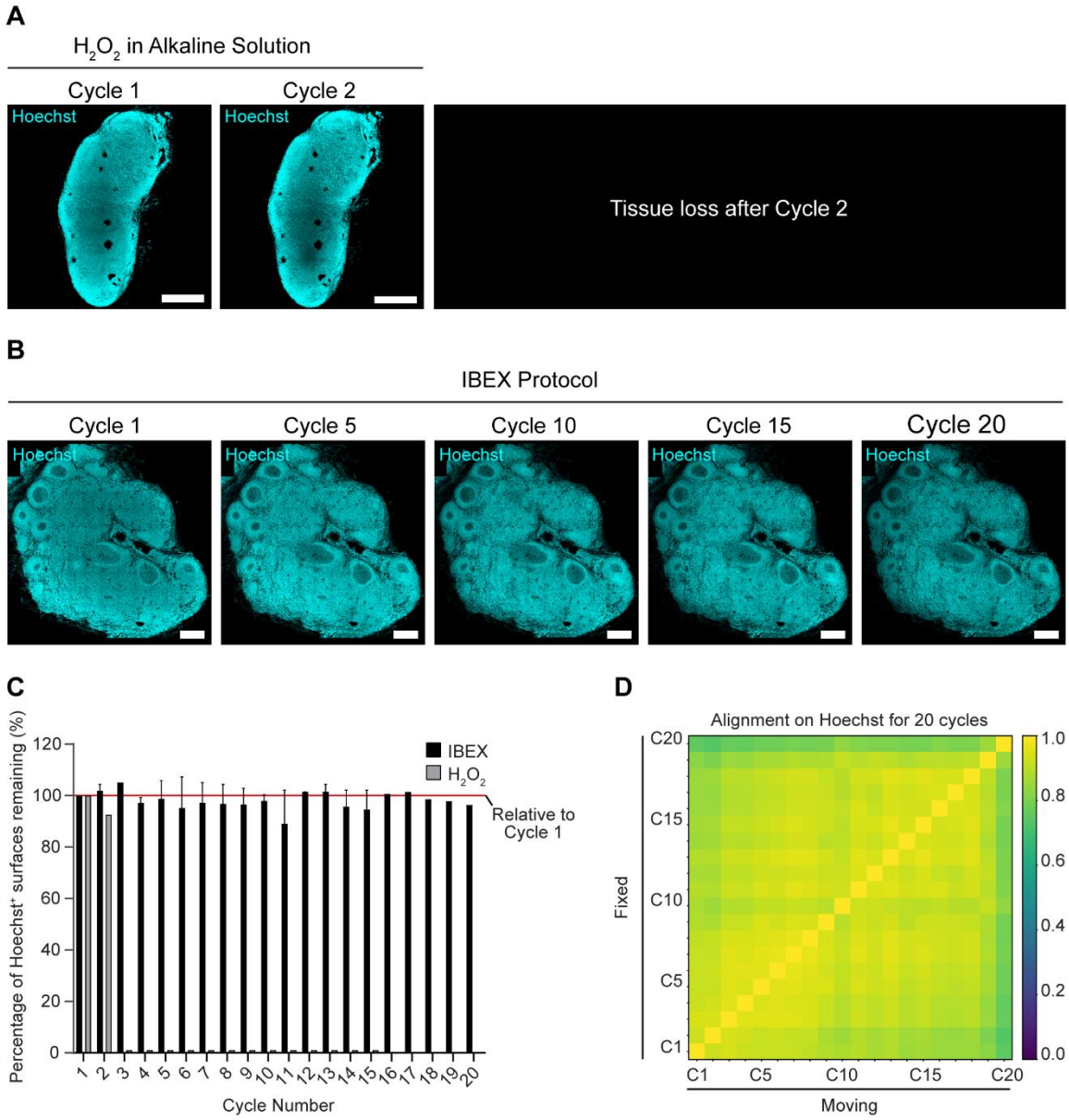

Figure S1. IBEX protocol preserves tissue integrity over high cycle number.

(A) Confocal images of mouse inguinal LN iteratively imaged using H_2O_2 in alkaline solution. Tissues lifted after 2 cycles and could not be imaged as a comparison. Scale bar corresponds to 500 µm. *(B)* Confocal images of human mesenteric LN iteratively imaged using IBEX protocol for 20 cycles. Scale bar corresponds to 500 µm. *(C)* Quantification of percentage of Hoechst+ surfaces remaining per cycle relative to the number of surfaces present in cycle 1. Red line is reflective of no tissue loss. Data are pooled from 2 similar experiments: a 15 cycle mouse inguinal LN and a 20 cycle human mesenteric LN. Shown is the mean ± SEM. *(D)* Cross correlation similarity matrix after alignment with Hoechst across 20 cycle experiment shown in B.

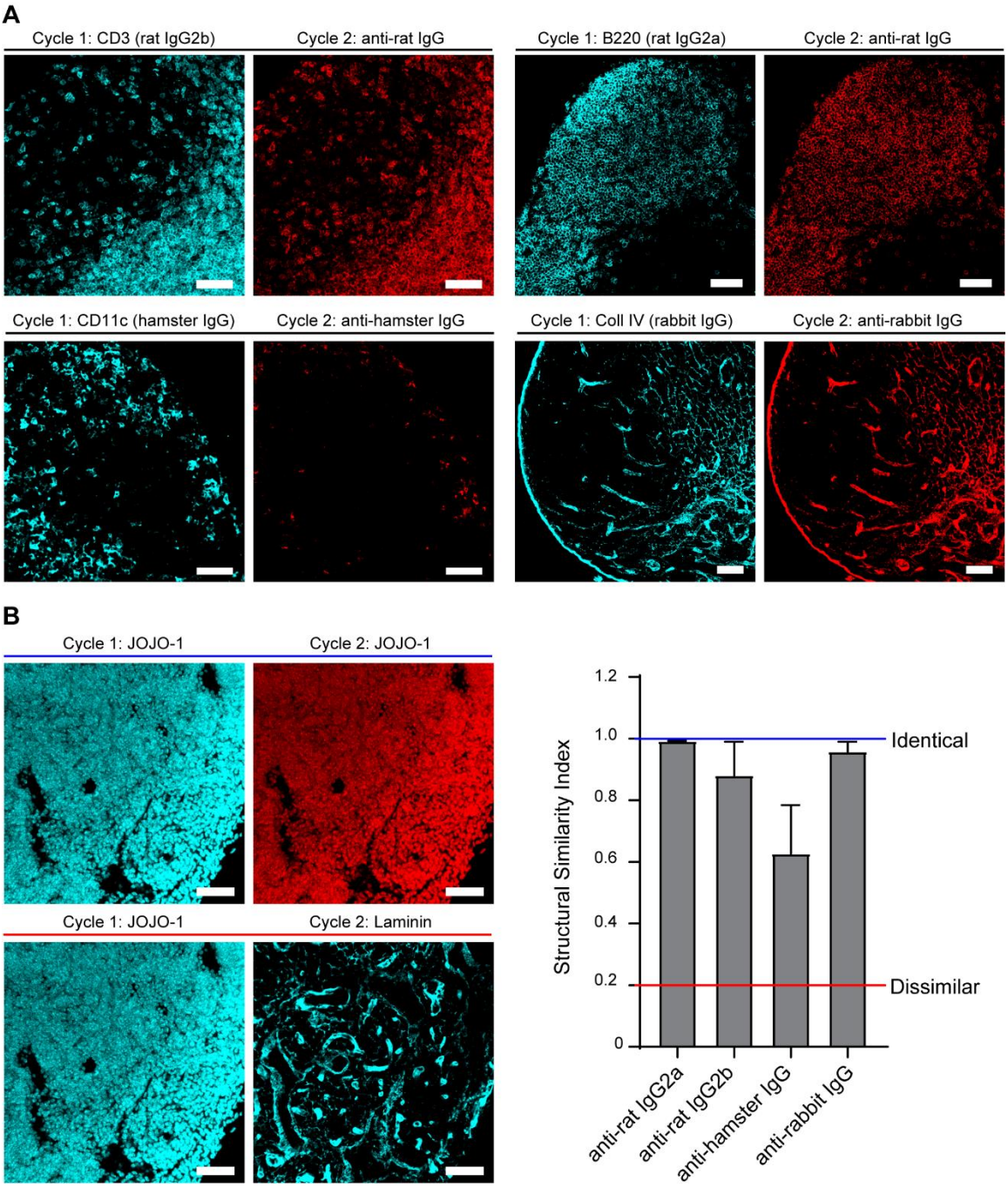

Figure S2. $LiBH_4$ primarily acts by bleaching fluorophores and not stripping antibodies.

Popliteal LN sections were stained with primary antibodies directed against various antigens, bleached with $LiBH_4$, and then labeled with secondary antibodies directed against the primary antibody isotype. *(A)* Confocal images of murine LN sections depicting the level of signal present with the primary antibodies as compared to an appropriate secondary antibody after IBEX protocol. *(B)* Bar graph summarizing the level of similarity between images captured before and after $LiBH_4$ treatment. Red line represents dissimilar images (Cycle 1 JOJO-1 versus Cycle 1 Laminin) and blue line denotes highly similar images (Cycle 1 JOJO-1 vs Cycle 2 JOJO-1). Data representative of 5 similar experiments. Shown is the mean ±SEM. Scale bar represents 50 µm.

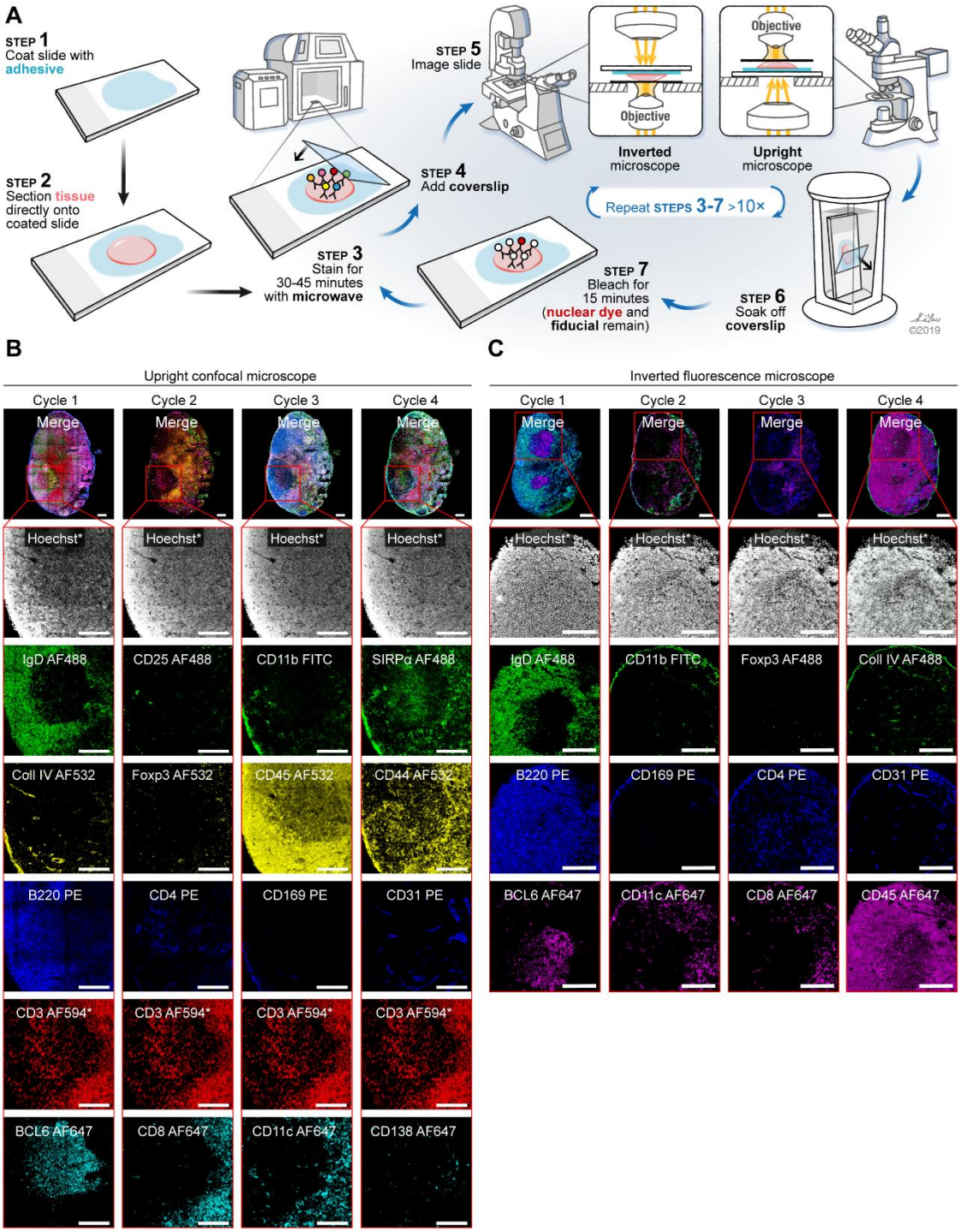

*Fiducials: Hoechst and CD3 AF594, scale bar 150 um

Figure S3. IBEX can be easily adapted to other microscope configurations.

(A) Schematic depicting IBEX protocol using an inverted or upright microscope. *(B)* Confocal images of popliteal LNs from SRBC-immunized mice. 30 µm tissue sections were labeled with 4 separate 6 parameter imaging panels. The nuclear dye Hoechst and membrane label CD3 AF594 were present throughout cycles 1-4 and served as fiducials. Top panels are a merge of all channels

for each cycle except for Hoechst. Scale bar represents 150 µm. Confocal images were acquired by an upright confocal microscope. (C) 5 µm sections from popliteal LNs from SRBC-immunized mice were visualized using an inverted epifluorescence microscope. Tissue sections were labeled with 4 separate 4 parameter imaging panels with Hoechst serving as a fiducial for cycles 1-4. Scale bar represents 150 µm.

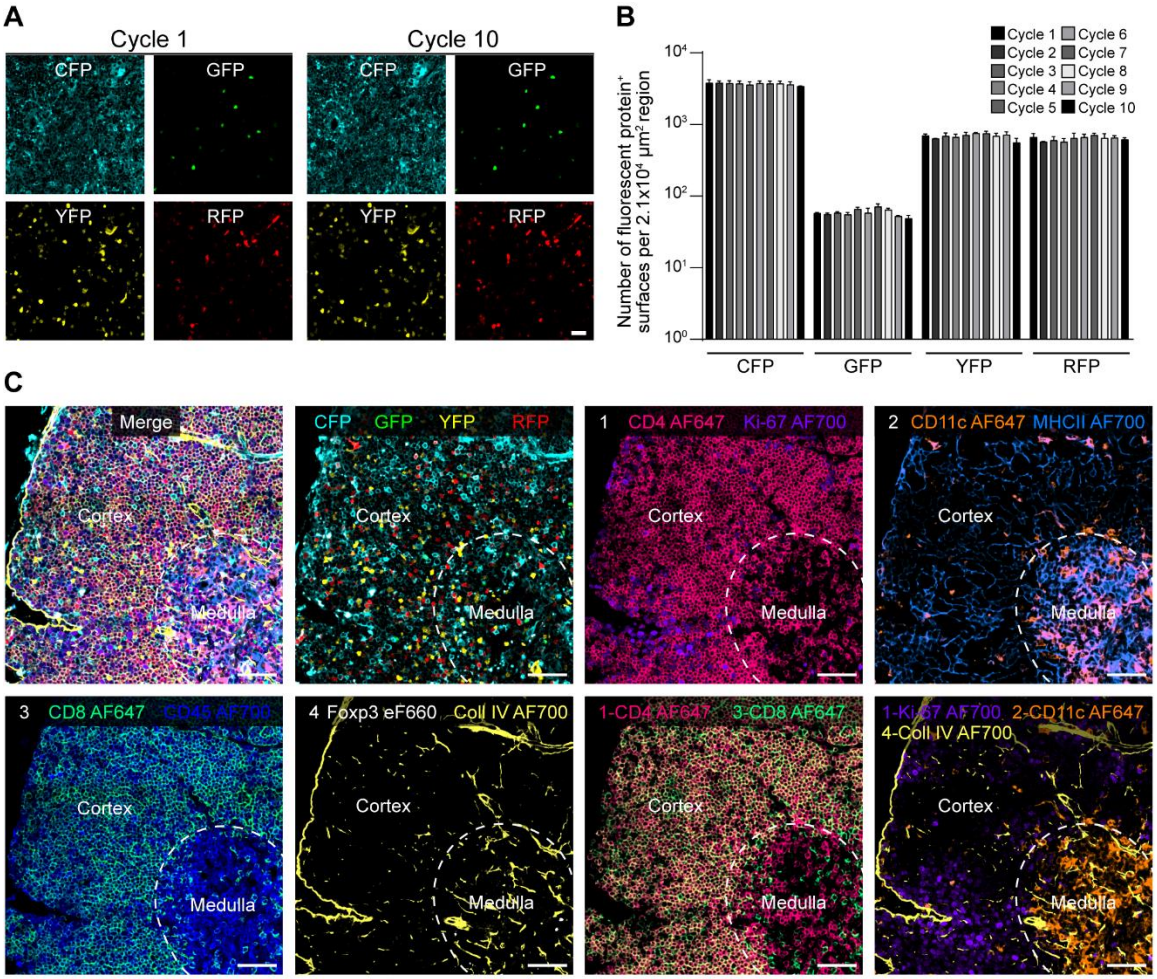

Figure S4. Fluorescent proteins are not bleached with IBEX protocol.

Fluorescent Confetti animals were injected i.p. with tamoxifen on day 0 and day 2 to induce the expression of the following fluorescent proteins: membrane CFP, nuclear GFP, and cytoplasmic YFP and RFP. On day 4, tissues were collected and processed for confocal microscopy. *(A)* Example images of signal from fluorescent proteins at Cycle 1 (no $LiBH_4$) and Cycle 10 (after 9 rounds of $LiBH_4$ bleaching). *(B)* Quantification of the number of fluorescent protein+ surfaces per $2.1x10^4$ μm^2 region of interest from 2 independent experiments. Shown is the mean ± SEM. *(C)* Four cycles of IBEX were applied to 30 µm sections of thymus tissue. AF647 and AF700 conjugated antibodies were used to stain immune and structural markers in the tissue. Representative images showing the compatibility of IBEX with transgenic animals expressing fluorescent proteins. Data are representative of 2 independent experiments. For A and C, images represent a single z slice and scale bar corresponds to 25 µm *(A)* or 50 µm *(B)*.

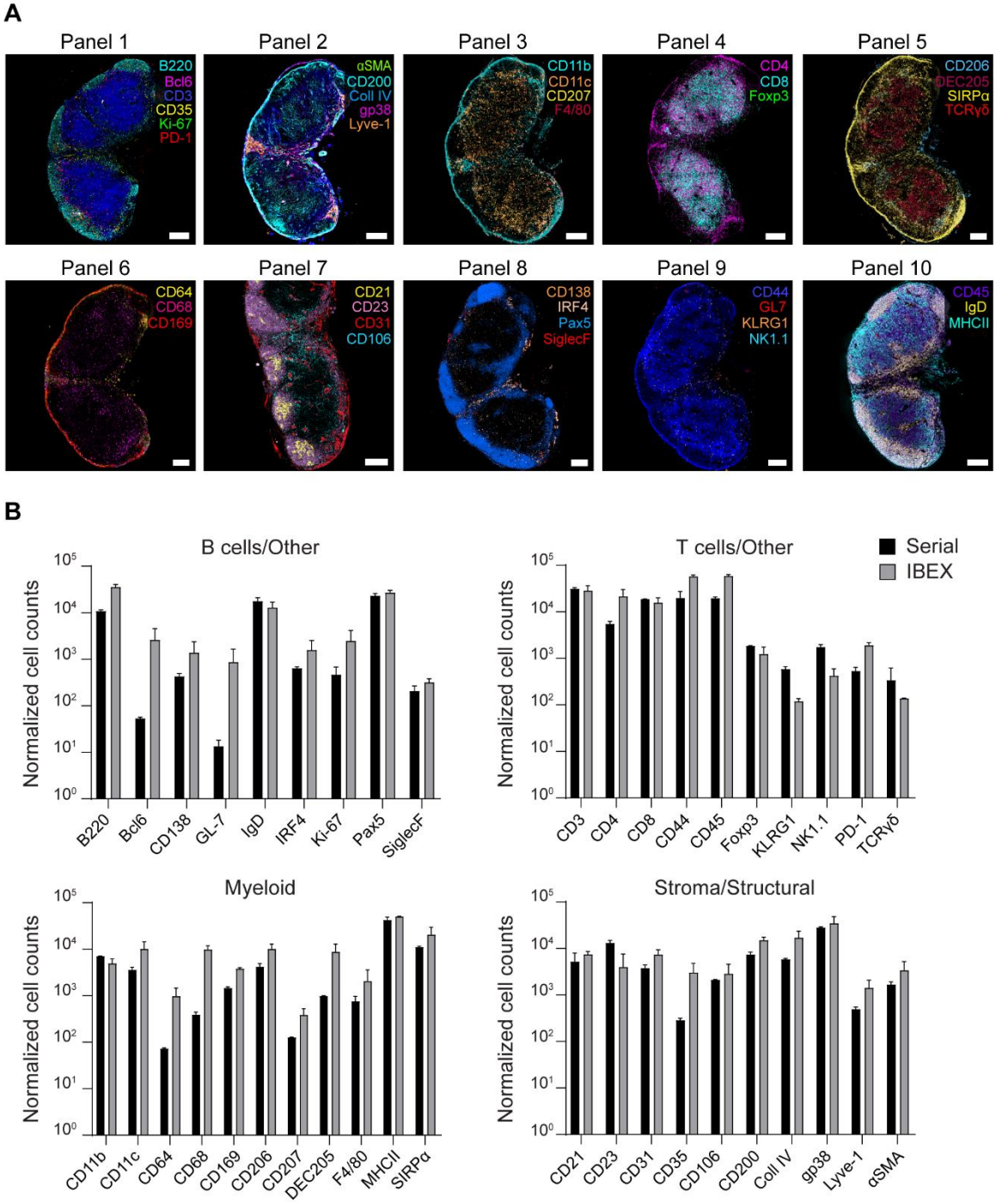

Figure S5. Comparable staining observed by serial and iterative immunofluorescence methods.

(A) Confocal images of inguinal LNs (iLNs) from SRBC-immunized mice. Serial sections were stained with the same panels used for the 10 cycle 41 parameter IBEX experiments described in Fig. 4A. Scale bar is 200 µm. (*B)* Cells were segmented on the nuclear marker JOJO-1 and the number of surfaces positive for each marker were quantified from images acquired serially as in A or iteratively via IBEX method. Data are from 2-3 LNs per group with 2 immunized iLNs for serial

method and 1 naïve pLN, 1 immunized pLN, and 1 immunized axillary LN (aLN) for IBEX method. Shown is the mean ± SEM. See Movie S7.

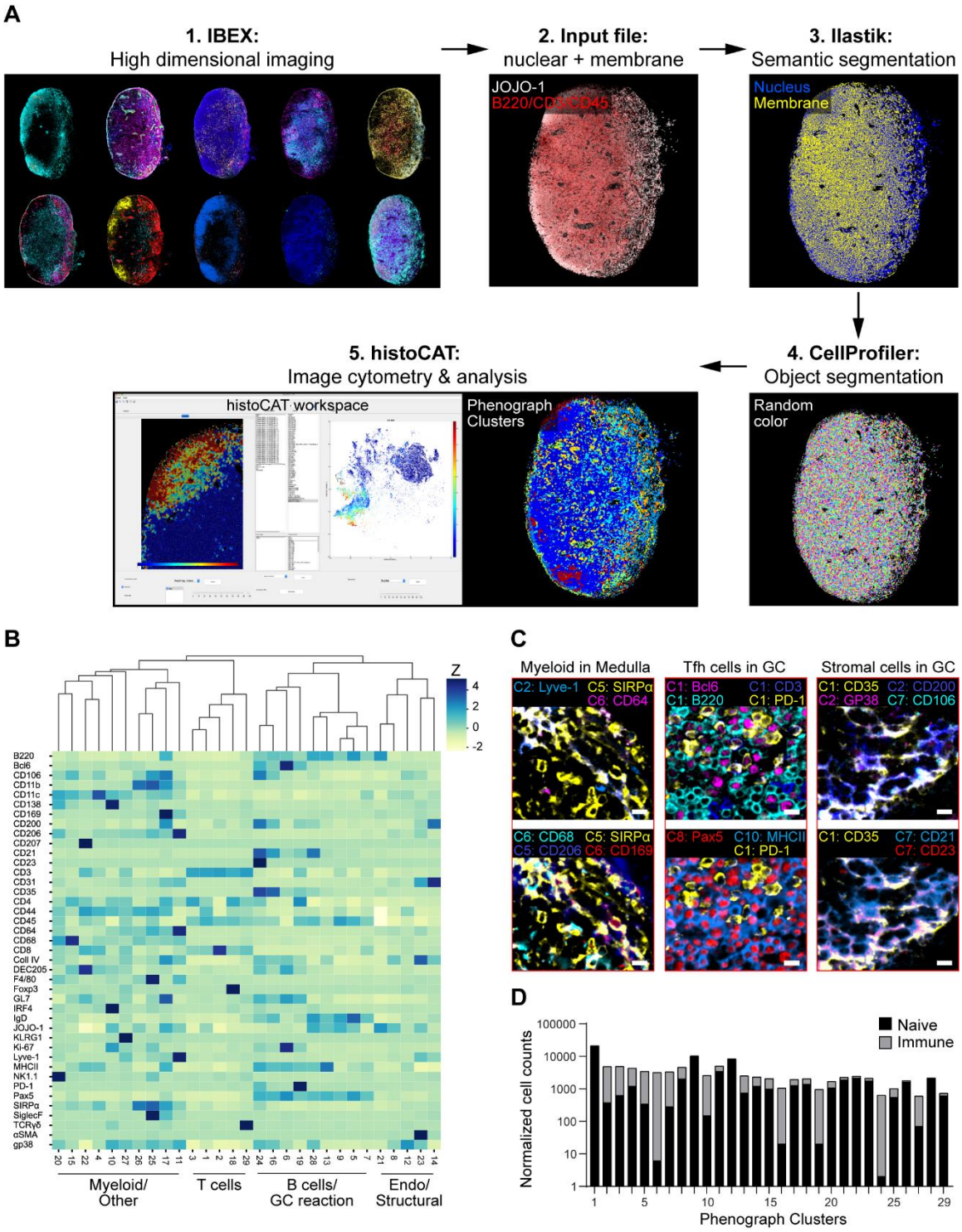

Figure S6. Data visualization and quantification with histoCAT.

(A) histoCAT workflow for image analysis. Step 1: High dimensional imaging of mouse LNs using IBEX method. Step 2: Nuclei were defined by JOJO-1 and membranes were generated by combining B220, CD3, and CD45 into one composite channel. Step 3: Semantic segmentation was performed using Ilastik. Step 4: Objects were further segmented using CellProfiler. Each

segmented cell is randomly colored and projected back onto original x-y coordinates. Step 5: Data visualization and analysis with histoCAT. (B) Marker expression heatmap for the phenotypes identified by PhenoGraph clustering in histoCAT using segmented cells from naïve (n = 32,091) and SRBC-immunized mouse LNs (n = 80,355). The heatmap displays relative expression levels based on Z-score normalized marker intensity values, and single cells are hierarchically clustered within each phenotype group. Numbers at the bottom of the heatmap indicate corresponding Phenograph cluster IDs with labels corresponding to manually assigned cell populations. Endothelial (Endo). *(C)* Example images of myeloid, Tfh, and stromal cell populations identified by histoCAT Phenograph clustering from an immunized mouse LN. Scale bar corresponds to 10 µm. *(D)* Normalized cell counts for Phenograph clusters obtained from naïve and SRBC-immunized mouse LNs. Data are from one experiment and are representative of 2 similar experiments.

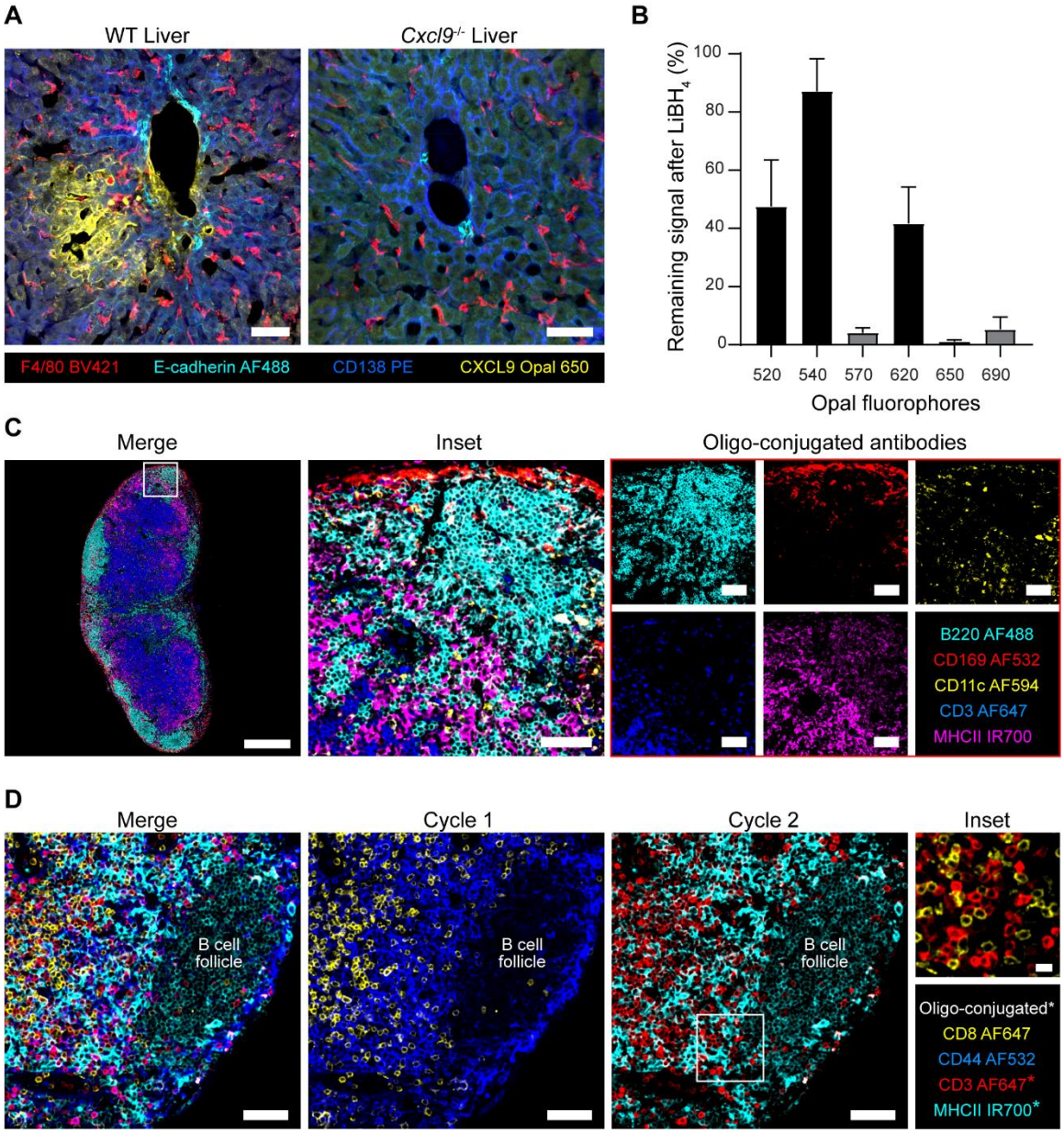

Figure S7. Extensions of IBEX workflow to enable single cell resolution of endogenous chemokines and immune populations using Opal fluorophores and oligonucleotide-conjugated antibodies.

(A) Detection of endogenous CXCL9 levels in fixed frozen mouse liver sections stained with indicated markers. Scale bars 50 µm. Confocal images are representative of 3 similar experiments. *(B)* Percentage of fluorophore signal remaining after 30 minutes of $LiBH_4$ treatment. Data are pooled from 4 experiments with iterative staining of the multiple Opal fluorophores. Shown is the mean ± SEM. *(C)* Confocal images of mouse inguinal LN labeled with 5 different oligo-conjugated antibodies and complementary fluorescent imager strands. Scale bars (left-most panel 400 µm or 100 µm). (*D)* Representative images from a 2 cycle IBEX experiment performed on inguinal mouse LNs where the first cycle consisted of fluorophore-conjugated antibodies and the second cycle consisted of oligo-conjugated antibodies denoted by the asterisks. Scale bars (50 µm, Inset 10 µm).

Tables S1-S5

Table S1. Time and method used to bleach fluorescently conjugated antibodies and dyes.

							Time to Bleach (Minutes)	
Marker	**Clone**	**Conjugate**	**Vendor**	**Cat No.**	**Isotype**	**Dilution**	$LiBH_4$	$LiBH_4$ + Light
β-3 Tubulin	AA10	BV421	BioLegend	657412	Mouse IgG2a, κ	1:200	-	<15
β-3 Tubulin	AA10	AF532	BioLegend	Custom	Mouse IgG2a, κ	1:100	<15	-
B220	RA3-6B2	BV421	BioLegend	103251	Rat IgG2a, κ	1:400	-	<15
B220	RA3-6B2	BV510	BioLegend	103248	Rat IgG2a, κ	1:300	-	<15
B220	RA3-6B2	AF488	BD Biosciences	557669	Rat IgG2a, κ	1:400	<15	-
B220	RA3-6B2	AF532	Thermo	58-0452-82	Rat IgG2a, κ	1:50	<15	-
B220	RA3-6B2	PE	BD Biosciences	553090	Rat IgG2a, κ	1:400	<15	-
B220	RA3-6B2	eF570	Thermo	41-0452-80	Rat IgG2a, κ	1:200	<15	-
B220	RA3-6B2	eF615	Thermo	42-0452-82	Rat IgG2a, κ	1:200	>120	-
B220	RA3-6B2	AF647	BioLegend	103226	Rat IgG2a, κ	1:400	<15	-
B220	RA3-6B2	AF700	BioLegend	103232	Rat IgG2a, κ	1:50	<15	-
BCL2	100	AF647	BioLegend	658705	Mouse IgG_1	1:25	<15	-
Bcl6	K112-91	AF647	BD Biosciences	561525	Mouse IgG_1, κ	1:50	<15	-
CD1c	L161	PE	BioLegend	331506	Mouse IgG_1, κ	1:50	<15	-
CD1d	1B1	PE	BD Biosciences	553846	Rat IgG2b, κ	1:100	<15	-
CD3	17A2	BV421	BioLegend	100228	Rat IgG2b, κ	1:400	-	<15
CD3	17A2	BV510	BioLegend	100234	Rat IgG2b, κ	1:50	-	<15
CD3	17A2	AF488	BioLegend	100210	Rat IgG2b, κ	1:200	<15	-
CD3	17A2	AF532	Thermo	58-0032-80	Rat IgG2b, κ	1:50	<15	-
CD3	17A2	PE	BioLegend	100205	Rat IgG2b, κ	1:200	<15	-
CD3	17A2	AF594	BioLegend	100240	Rat IgG2b, κ	1:400	>120	-
CD3	17A2	AF647	BD Biosciences	557869	Rat IgG2b, κ	1:400	<15	-
CD3	UCHT1	AF532	Thermo	58-0038-42	Mouse IgG_1, κ	1:50	<15	-
CD3	UCHT1	AF594	BioLegend	300446	Mouse IgG_1	1:200	>120	-
CD4	GK1.5	BV421	BioLegend	100443	Rat IgG2b, κ	1:200	-	<15
CD4	GK1.5	BV510	BioLegend	100449	Rat IgG2b, κ	1:50	-	<15
CD4	GK1.5	PE	BD Biosciences	553730	Rat IgG2b, κ	1:200	<15	-
CD4	GK1.5	AF594	BioLegend	100446	Rat IgG2b, κ	1:200	>120	-
CD4	RM4-5	AF488	BD Biosciences	557667	Rat IgG2a, κ	1:100	<15	-
CD4	RM4-5	AF532	Thermo	58-0042-80	Rat IgG2a, κ	1:50	<15	-
CD4	RM4-5	eF570	Thermo	41-0042-82	Rat IgG2a, κ	1:100	<15	-
CD4	RPA-T4	AF532	Thermo	58-0049-42	Mouse IgG_1, κ	1:25	<15	-
CD4	RPA-T4	AF700	BioLegend	300526	Mouse IgG_1, κ	1:25	<15	-
CD8	53-6.7	BV421	BioLegend	100738	Rat IgG2a, κ	1:200	-	<15
CD8	53-6.7	BV510	BioLegend	100752	Rat IgG2a, κ	1:200	-	<15
CD8	53-6.7	AF488	BioLegend	100723	Rat IgG2a, κ	1:200	<15	-
CD8	53-6.7	PE	BD Biosciences	553032	Rat IgG2a, κ	1:400	<15	-
CD8	53-6.7	AF594	BioLegend	100758	Rat IgG2a, κ	1:200	>120	-
CD8	53-6.7	AF647	BioLegend	100724	Rat IgG2a, κ	1:200	<15	-
CD8	SK1	AF488	BioLegend	344716	Mouse IgG_1, κ	1:50	<15	-
CD10	FR4D11	PE	Caprico Biotechnologies	103926	Mouse IgG_1, κ	1:50	<15	-
CD11b	5C6	FITC	Bio-Rad	MCA711F	Rat IgG2b	1:100	<15	-
CD11b	5C6	PE	Bio-Rad	MCA711PE	Rat IgG2b	1:100	<15	-
CD11b	M1/70	AF488	BioLegend	101217	Rat IgG2b, κ	1:100	<15	-
CD11c	N418	AF488	Thermo	MCD11c20	Hamster IgG	1:50	<15	-
CD11c	N418	AF594	BioLegend	117346	Hamster IgG	1:50	>120	-
CD11c	N418	AF647	BioLegend	117312	Hamster IgG	1:100	<15	-
CD11c	B-Ly6	AF700	BD Biosciences	561352	Mouse IgG_1, κ	1:25	<15	-
CD20	L26	AF488	Thermo	53-0202-82	Mouse IgG2b, κ	1:200	<15	-
CD21	7E9	Pacific Blue	BioLegend	123413	Rat IgG2a, κ	1:200	<15	-
CD21	Bu32	AF532	BioLegend	Custom	Mouse IgG_1, κ	1:400	<15	-
CD23	B3B4	AF647	BioLegend	101611	Rat IgG2a, κ	1:50	<15	-
CD23	EBVCS-5	AF532	BioLegend	NA, Custom	Mouse IgG_1, κ	1:25	<15	-
CD25	PC61.5	AF488	Thermo	53-0251-82	Rat IgG1, λ	1:50	<15	-
CD25	M-A251	AF647	BioLegend	356127	Mouse IgG_1, κ	1:50	<15	-

CD31	MEC13.3	AF488	BioLegend	102514	Rat IgG2a, κ	1:100	<15	-
CD31	MEC13.3	PE	BD Biosciences	553373	Rat IgG2a, κ	1:200	<15	-
CD31	MEC13.3	AF594	BioLegend	102520	Rat IgG2a, κ	1:100	>120	-
CD31	MEC13.3	AF647	BioLegend	102516	Rat IgG2a, κ	1:100	<15	-
CD31	WM59	AF700	BioLegend	303133	Mouse IgG_1, κ	1:25	<15	-
CD34	QBEND/10	PE	Thermo	MAI-10205	Mouse IgG_1	1:50	<15	-
CD35	8C12	BV510	BD Biosciences	740132	Rat IgG2a, κ	1:600	-	<15
CD35	E11	PE	BioLegend	333406	Mouse IgG_1, κ	1:800	<15	-
CD38	HIT2	AF700	BioLegend	303524	Mouse IgG_1, κ	1:25	<15	-
CD39	A1	PE	BioLegend	328208	Mouse IgG_1, κ	1:50	<15	-
CD44	IM7	AF488	BioLegend	103016	Rat IgG2b, κ	1:100	<15	-
CD44	IM7	AF532	BioLegend	Custom	Rat IgG2b, κ	1:100	<15	-
CD44	IM7	AF647	BioLegend	103018	Rat IgG2b, κ	1:100	<15	-
CD44	IM7	AF700	BioLegend	103026	Rat IgG2b, κ	1:50	<15	-
CD45	30-F11	BV421	BioLegend	103134	Rat IgG2b, κ	1:100	-	<15
CD45	30-F11	BV510	BioLegend	103138	Rat IgG2b, κ	1:100	-	<15
CD45	30-F11	AF488	BioLegend	103122	Rat IgG2b, κ	1:200	<15	-
CD45	30-F11	AF532	Thermo	58-0451-82	Rat IgG2b, κ	1:200	<15	-
CD45	30-F11	AF647	BioLegend	103124	Rat IgG2b, κ	1:400	<15	-
CD45	30-F11	AF700	BioLegend	103128	Rat IgG2b, κ	1:50	<15	-
CD45	HI30	AF532	Thermo	58-0459-41	Mouse IgG_1, κ	1:50	<15	-
CD45	F10-89-4	PE/iFluor594	Caprico Biotechnologies	1016185	Mouse IgG2a, κ	1:50	<15	-
CD49a	TS2/7	PE	BioLegend	328304	Mouse IgG_1, κ	1:50	<15	-
CD54	HA58	AF647	BioLegend	353114	Mouse IgG_1, κ	1:50	<15	-
CD64	X54-5/7.1	AF647	BioLegend	139322	Mouse IgG_1, κ	1:50	<15	-
CD66b	G10F5	AF647	BioLegend	305110	Mouse IgM, κ	1:25	<15	-
CD68	FA-11	BV421	BioLegend	137017	Rat IgG2a	1:200	-	<15
CD68	FA-11	AF488	BioLegend	137011	Rat IgG2a	1:50	<15	-
CD68	KP1	AF647	Santa Cruz	sc-200060	Mouse IgG_1, κ	1:100	<15	-
CD69	-	None	R&D	AF2386	Goat IgG	1:50	-	-
CD69	H1.2F3	PE	BioLegend	104508	Hamster IgG	1:50	<15	-
CD69	FN50	AF647	BioLegend	310918	Mouse IgG_1, κ	1:100	<15	-
CD94	DX22	PE	BioLegend	305506	Mouse IgG_1, κ	1:50	<15	-
CD103	2E7	AF488	BioLegend	121407	Hamster IgG	1:100	<15	-
CD106	429	AF488	BioLegend	105710	Rat IgG2a, κ	1:50	<15	-
CD106	429	eF660	Thermo	50-1061-80	Rat IgG2a, κ	1:50	<15	-
CD106	STA	PE	BioLegend	305806	Mouse IgG_1, κ	1:50	<15	-
CD117	2B8	BV421	BioLegend	105827	Rat IgG2b, κ	1:50	-	<15
CD117	104D2	AF488	BioLegend	313234	Mouse IgG_1, κ	1:50	<15	-
CD138	281-2	BV421	BD Biosciences	562610	Rat IgG2a, κ	1:50	-	<15
CD138	281-2	AF647	BioLegend	142526	Rat IgG2a, κ	1:50	<15	-
CD138	MI15	PE	BioLegend	356504	Mouse IgG_1, κ	1:200	<15	-
CD138	MI15	AF647	BioLegend	356523	Mouse IgG_1, κ	1:200	<15	-
CD163	GH1/61	AF647	BioLegend	333620	Mouse IgG_1, κ	1:100	<15	-
CD166	EPR2759	AF488	AbCAM	Ab197543	Rabbit mAb	1:100	<15	-
CD169	3D6.112	FITC	Bio-Rad	MCA884F	Rat IgG2a, κ	1:50	<15	-
CD169	3D6.112	PE	Biolegend	142404	Rat IgG2a, κ	1:300	<15	-
CD169	3D6.112	AF594	BioLegend	142416	Rat IgG2a, κ	1:100	>120	-
CD200	Ox-90	BV421	BD Biosciences	565547	Rat IgG2a, κ	1:100	-	<15
CD206	C068C2	BV421	BioLegend	141717	Rat IgG2a, κ	1:100	-	<15
CD207	eBioL31	PE	Thermo	12-2075-80	Rat IgG2a	1:50	<15	-
Clec9a	8F9	AF488	BioLegend	Custom	Mouse IgG2a, κ	1:25	<15	-
Collagen IV	-	None	AbCAM	19808	Rabbit IgG	1:200	-	-
Collagen IV	-	None	AbCAM	Ab6586	Rabbit IgG	1:200	-	-
CXCL12	79018	AF532	R&D	MAB350-500 (Unconjugated)	Mouse IgG_1	1:25	<15	-
CXCL13	-	AF532	R&D	AF801 (Unconjugated)	Goat IgG	1:25	<15	-
CXCR6	221002	AF647	Novus	FAB2145R	Rat IgG2b	1:50	<15	-
Cytokeratin	C-11	AF647	BioLegend	628604	Mouse IgG_1, κ	1:200	<15	-
Cytokeratin	AE1/AE3	eF660	Thermo	50-9003-82	Mouse IgG_1	1:100	<15	-
DCAMKL1	-	None	AbCAM	Ab37994	Rabbit IgG	1:50	-	-

DC-SIGN	9E9A8	AF647	BioLegend	330112	Mouse IgG2a, κ	1:50	<15	-
DEC205	NLDC-145	AF647	BioLegend	138204	Rat IgG2a, κ	1:50	<15	-
Desmin	-	None	AbCAM	Ab15200	Rabbit IgG	1:200	-	-
Desmin	Y66	AF488	AbCAM	Ab185033	Rabbit IgG	1:200	<15	-
E-cadherin	DECMA-1	AF647	BioLegend	147308	Rat IgG1, κ	1:100	<15	-
EpCAM	G8.8	BV510	BD Biosciences	563216	Rat IgG2a, κ	1:100	-	<15
EpCAM	G8.8	AF594	BioLegend	118222	Rat IgG2a, κ	1:400	>120	-
EpCAM	G8.8	AF647	BioLegend	118212	Rat IgG2a, κ	1:200	<15	-
EpCAM	9C4	AF594	BioLegend	324228	Mouse IgG2b, κ	1:500	>120	-
EpCAM	9C4	AF647	BioLegend	324212	Mouse IgG2b, κ	1:100	<15	-
F4/80	BM8	BV421	BioLegend	123132	Rat IgG2a, κ	1:50	-	<15
F4/80	BM8	PE	Thermo	12-4801-82	Rat IgG2a, κ	1:100	<15	-
F4/80	BM8	AF647	BioLegend	123122	Rat IgG2a, κ	1:50	<15	-
F4/80	BM8	AF700	BioLegend	123130	Rat IgG2a, κ	1:50	<15	-
Fibronectin	2F4	AF532	Novus	NBP2-22113AF532	Mouse IgG_1	1:25	<15	-
Foxp3	FJK-16s	AF488	Thermo	53-5773-82	Rat IgG2a, κ	1:50	<15	-
Foxp3	FJK-16s	AF532	Thermo	58-5773-82	Rat IgG2a, κ	1:50	<15	-
Foxp3	FJK-16s	PE	Thermo	12-5773-82	Rat IgG2a, κ	1:50	<15	-
Foxp3	FJK-16s	eF570	Thermo	41-5773-82	Rat IgG2a, κ	1:50	<15	-
Foxp3	FJK-16s	eF660	Thermo	50-5773-82	Rat IgG2a, κ	1:50	<15	-
FOXP3	236A/E7	eF570	Thermo	41-4777-82	Mouse IgG_1, κ	1:50	<15	-
GL-7	GL7	PE	BD Biosciences	561530	Rat IgM, κ	1:100	<15	-
Glutamine synthetase	-	None	AbCAM	Ab49873	Rabbit IgG	1:200	-	-
gp38	8.1.1	AF488	BioLegend	127405	Hamster IgG	1:50	<15	-
HLA-DR	L243	AF488	BioLegend	307619	Mouse IgG2a, κ	1:200	<15	-
Hoechst	-	-	Biotium	40046	-	1:5,000	-	-
ICOS	CS98.4A	AF488	BioLegend	313514	Hamster IgG	1:25	<15	-
IgA	-	AF555	Southern Biotech	1040-32	Goat IgG	1:500	<15	-
IgA1	B3506B4	AF647	SouthernBiotech	9130-31	Mouse IgG_1, κ	1:500	<15	-
IgA2	A9604D2	AF488	SouthernBiotech	9140-30	Mouse IgG_1, κ	1:500	<15	-
IgD	11-26c.2a	AF488	BioLegend	405718	Rat IgG2a, κ	1:400	<15	-
IgD	11-26c.2a	AF594	BioLegend	405740	Rat IgG2a, κ	1:400	>120	-
IgD	11-26c.2a	AF700	BioLegend	405729	Rat IgG2a, κ	1:50	<15	-
IgD	IA6-2	AF488	BioLegend	348216	Mouse IgG2a, κ	1:25	<15	-
IgM	EPR5539-65-4	AF647	AbCAM	Ab200629	Rabbit mAb	1:100	<15	-
IRF4	3E4	FITC	Thermo	11-9858-82	Rat IgG1, κ	1:50	<15	-
IRF4	3E4	PE	Thermo	12-9858-82	Rat IgG1, κ	1:50	<15	-
JOJO-1	-	-	Thermo	J11372	-	1:10,000	-	-
Keratin 14	Poly9060	-	BioLegend	906004	Chicken IgY	1:50	-	-
Keratin 18	1G11C4	CoraLite488	ProteinTech	CL488-66187	Mouse IgG_1	1:50	<15	-
Ki-67	B56	AF488	BD Biosciences	558616	Mouse IgG_1, κ	1:50	<15	-
Ki-67	B56	AF700	BD Biosciences	561277	Mouse IgG_1, κ	1:50	<15	-
KLRG1	2F1	AF488	BD Biosciences	561619	Hamster IgG_2, κ	1:50	<15	-
Laminin 1 + 2	-	None	AbCAM	Ab7463	Rabbit IgG	1:100	-	-
Lumican	-	AF532	R&D	AF2846 (Unconjugated)	Goat IgG	1:50	<15	-
Ly-6G	1A8	AF488	BioLegend	127626	Rat IgG2a, κ	1:50	<15	-
Lysozyme	-	-	AbCAM	Ab2408	Rabbit IgG	1:50	-	-
Lyve-1	ALY7	eF570	Thermo	41-0443-82	Rat IgG1, κ	1:100	<15	-
Lyve-1	-	AF532	R&D	AF2089 (Unconjugated)	Goat IgG	1:100	<15	-
MARCO	-	-	Thermo	PA5-64134	Rabbit IgG	1:25	-	-
MHC-II	M5/114.15.2	BV421	BioLegend	107631	Rat IgG2b, κ	1:400	-	<15
MHC-II	M5/114.15.2	AF647	BioLegend	107618	Rat IgG2b, κ	1:600	<15	-
MHC-II	M5/114.15.2	AF700	BioLegend	107622	Rat IgG2b, κ	1:100	<15	-
NF-H/NF-M	SM1-35	AF488	BioLegend	835614	Mouse IgG_1, κ	1:50	<15	-
NK1.1	PK136	BV421	BioLegend	108731	Mouse IgG2a, κ	1:50	-	<15
p53	PAb 240	PE	Novus	NB200-103PE	Mouse IgG_1, κ	1:50	<15	-
Pax5	1H9	AF647	BioLegend	649704	Rat IgG2a, κ	1:100	<15	-
PD-1	29F.1A.12	BV421	BioLegend	135217	Rat IgG2a, κ	1:100	-	<15
PD-1	29F.1A.12	PE	BioLegend	135206	Rat IgG2a, κ	1:100	<15	-
PD-1	EH12.2H7	PE	BioLegend	329906	Mouse IgG_1, κ	1:200	<15	-
RoRyt	AFKJS-9	-	Thermo	14-6988-82	Rat IgG2a	1:200	-	-

SiglecF	E50-2440	PE	BD Biosciences	552126	Rat IgG2a, κ	1:100	<15	-
SiglecF	1RNM44N	AF700	Thermo	56-1702-80	Rat IgG2a, κ	1:50	<15	-
SIRPα	P84	AF488	BioLegend	144024	Rat IgG1, κ	1:50	<15	-
SIRPα	P84	AF647	BioLegend	144027	Rat IgG1, κ	1:200	<15	-
αSMA	1A4	AF488	Thermo	53-9760-80	Mouse IgG2a, κ	1:500	<15	-
αSMA	1A4	eF660	Thermo	53-9760-82	Mouse IgG2a, κ	1:500	<15	-
SPARC	-	AF532	R&D	AF941 (Unconjugated)	Goat IgG	1:50	<15	-
TCRγδ	GL3	AF488	BioLegend	118128	Hamster IgG	1:50	<15	-
TCRγδ	GL3	PE	BioLegend	118108	Hamster IgG	1:100	<15	-
TCRγδ	B1	PE	BioLegend	331210	Mouse IgG_1, κ	1:100	<15	-
Tim-3	344823	AF532	R&D	MAB2365 (Unconjugated)	Rat IgG2a	1:25	<15	-
Tim-4	21H12	BV421	BD Biosciences	742773	Rat IgG1, κ	1:100	-	<15
Tryptase	AA1	-	AbCAM	Ab2378	Mouse IgG_1	1:50	<15	-
Vα7.2	3C10	AF647	BioLegend	351726	Mouse IgG_1, κ	1:50	<15	-
Vimentin	O91D3	AF532	BioLegend	Custom	Mouse IgG2a	1:200	<15	-
anti-chicken IgY	-	FITC	Thermo	SA1-72000	Donkey IgG	1:200	<15	-
anti-goat IgG	-	AF488	Thermo	A-11055	Donkey IgG	1:400	<15	-
anti-hamster IgG	-	AF647	Thermo	A-21451	Goat IgG	1:400	<15	-
anti-rabbit IgG	-	AF488	Thermo	A-11034	Goat IgG	1:400	<15	-
anti-rabbit IgG	-	AF532	Thermo	A-11009	Goat IgG	1:400	<15	-
anti-rabbit IgG	-	AF555	Thermo	A-21428	Goat IgG	1:400	<15	-
anti-rabbit IgG	-	AF594	Thermo	A-11037	Goat IgG	1:400	>120	-
anti-rabbit IgG	-	AF647	Thermo	A-21245	Goat IgG	1:400	<15	-
anti-rabbit IgG	-	AF700	Thermo	A-21038	Goat IgG	1:400	<15	-
anti-rabbit IgG	-	AF750	Thermo	A-21039	Goat IgG	1:400	<15	-
anti-rabbit IgG	-	AF647	Thermo	A-31573	Donkey IgG	1:400	<15	-
anti-rabbit IgG	-	AF488	Thermo	Z25302	Goat Fab_2	-	<15	-
anti-rabbit IgG	-	AF532	Thermo	Z25303	Goat Fab_2	-	<15	-
anti-rabbit IgG	-	AF555	Thermo	Z25305	Goat Fab_2	-	<15	-
anti-rabbit IgG	-	AF594	Thermo	Z25307	Goat Fab_2	-	>120	-
anti-rabbit IgG	-	AF647	Thermo	Z25308	Goat Fab_2	-	<15	-
anti-rat IgG	-	AF647	Thermo	A-21247	Goat IgG	1:400	<15	-

Table S2. IBEX panels for individual organs (See Figs. 3, 4A, and Movies S1-S7).

Spleen: 16 parameters, 3 cycles

Cycle	Marker	Clone	Conjugate	Vendor	Catalog Number	Dilution
1	CD8	53-6.7	BV421	BioLegend	100738	1:200
	Autofluorescence	-	BV510*	-	-	-
	Autofluorescence	-	AF488**	-	-	-
	B220	RA3-6B2	PE	BD Biosciences	553090	1:400
	CD4	GK1.5	AF594	BioLegend	100446	1:200
	Foxp3	FJK-16s	eF660	Thermo	50-5773-82	1:50
	IgD	11-26c.2a	AF700	BioLegend	405729	1:50
2	F4/80	BM8	BV421	BioLegend	123132	1:50
	Autofluorescence	-	BV510*	-	-	-
	Collagen IV Goat anti-rabbit IgG	- -	None AF488	AbCAM Thermo	19808 A-11034	1:200 1:400
	CD169	3D6.112	PE	Biolegend	142404	1:300
	CD4	GK1.5	AF594	BioLegend	100446	1:200
	CD11c	N418	AF647	BioLegend	117312	1:100
	MHC-II	M5/114.15.2	AF700	BioLegend	107622	1:100
3	CD68	FA-11	BV421	BioLegend	137017	1:200
	Autofluorescence	-	BV510*	-	-	-
	CD45	30-F11	AF488	BioLegend	103122	1:50
	CD31	MEC13.3	PE	BD Biosciences	553373	1:200
	JOJO-1	-	AF532	Thermo	J11372	1:20,000
	CD4	GK1.5	AF594	BioLegend	100446	1:200
	CD3	17A2	AF647	BD Biosciences	557869	1:400
	Ki-67	B56	AF700	BD Biosciences	561277	1:50

Thymus: 26 parameters, 5 cycles

Cycle	Marker	Clone	Conjugate	Vendor	Catalog Number	Dilution
1	CD138	281-2	BV421	BD Biosciences	562610	1:50
	CD11b	5C6	FITC	Bio-Rad	MCA711F	1:100
	β-3 Tubulin	AA10	AF532	BioLegend	Custom	1:100
	B220	RA3-6B2	PE	BD Biosciences	553090	1:400
	CD3	17A2	AF594	BioLegend	100240	1:400
	CD106	429	eF660	Thermo	50-1061-80	1:50
	Collagen IV Goat anti-rabbit IgG	- -	None AF700	AbCAM Thermo	19808 A-21038	1:200 1:400
2	CD8	53-6.7	BV421	BioLegend	100738	1:200
	CD25	PC61.5	AF488	Thermo	53-0251-82	1:50
	Foxp3	FJK-16s	AF532	Thermo	58-5773-82	1:50
	CD4	RM4-5	eF570	Thermo	41-0042-82	1:100
	CD3	17A2	AF594	BioLegend	100240	1:400
	DEC205	NLDC-145	AF647	BioLegend	138204	1:50
	Ki-67	B56	AF700	BD Biosciences	561277	1:50
3	CD68	FA-11	BV421	BioLegend	137017	1:200
	SIRPα	P84	AF488	BioLegend	144024	1:50
	CD31	MEC13.3	PE	BD Biosciences	553373	1:200
	CD3	17A2	AF594	BioLegend	100240	1:400
	CD11c	N418	AF647	BioLegend	117312	1:100
	MHC-II	M5/114.15.2	AF700	BioLegend	107622	1:100
4	CD206	C068C2	BV421	BioLegend	141717	1:100
	αSMA	1A4	AF488	Thermo	53-9760-80	1:500
	CD44	IM7	AF532	BioLegend	Custom	1:100
	CD169	3D6.112	PE	Biolegend	142404	1:300
	CD3	17A2	AF594	BioLegend	100240	1:400
	CD45	30-F11	AF700	BioLegend	103128	1:50
5	JOJO-1	-	AF532	Thermo	J11372	1:20,000
	TCRγδ	GL3	PE	BioLegend	118108	1:100
	CD3	17A2	AF594	BioLegend	100240	1:400
	Cytokeratin	C-11	AF647	BioLegend	628604	1:200

Lung: 23 parameters, 4 cycles

Cycle	Marker	Clone	Conjugate	Vendor	Catalog Number	Dilution
1	CD206	C068C2	BV421	BioLegend	141717	1:100
	CD11b	5C6	FITC	Bio-Rad	MCA711F	1:100
	CD4	RM4-5	AF532	Thermo	58-0042-80	1:50
	Lyve-1	ALY7	eF570	Thermo	41-0443-82	1:100

	CD31	MEC13.3	AF594	BioLegend	102520	1:100
	CD11c	N418	AF647	BioLegend	117312	1:100
	SiglecF	1RNM44N	AF700	Thermo	56-1702-80	1:50
2	CD68	FA-11	BV421	BioLegend	137017	1:200
	Ly-6G	1A8	AF488	BioLegend	127626	1:50
	β-3 Tubulin	AA10	AF532	BioLegend	Custom	1:100
	B220	RA3-6B2	PE	BD Biosciences	553090	1:400
	CD31	MEC13.3	AF594	BioLegend	102520	1:100
	EpCAM	G8.8	AF647	BioLegend	118212	1:200
	MHC-II	M5/114.15.2	AF700	BioLegend	107622	1:100
3	CD138	281-2	BV421	BD Biosciences	562610	1:50
	KLRG1	2F1	AF488	BD Biosciences	561619	1:50
	IgA	-	AF555	Southern Biotech	1040-32	1:500
	CD31	MEC13.3	AF594	BioLegend	102520	1:100
	CD44	IM7	AF647	BioLegend	103018	1:100
	Collagen IV Goat anti-rabbit IgG	- -	None AF700	AbCAM Thermo	19808 A-21038	1:200 1:400
4	αSMA	1A4	AF488	Thermo	53-9760-80	1:500
	JOJO-1	-	AF532	Thermo	J11372	1:20,000
	CD169	3D6.112	PE	Biolegend	142404	1:300
	CD31	MEC13.3	AF594	BioLegend	102520	1:100
	CD8	53-6.7	AF647	BioLegend	100724	1:200
	CD45	30-F11	AF700	BioLegend	103128	1:50

Small Intestine: 20 parameters, 3 cycles

Cycle	Marker	Clone	Conjugate	Vendor	Catalog Number	Dilution
1	CD8	53-6.7	BV421	BioLegend	100738	1:200
	CD35	8C12	BV510	BD Biosciences	740132	1:600
	CD4	RM4-5	AF532	Thermo	58-0042-80	1:50
	Foxp3	FJK-16s	eF570	Thermo	41-5773-82	1:50
	EpCAM	G8.8	AF594	BioLegend	118222	1:400
	CD3	17A2	AF647	BD Biosciences	557869	1:400
	IgD	11-26c.2a	AF700	BioLegend	405729	1:50
2	CD117	2B8	BV421	BioLegend	105827	1:50
	B220	RA3-6B2	BV510	BioLegend	103248	1:300
	KLRG1	2F1	AF488	BD Biosciences	561619	1:50
	DCAMKL1 Goat anti-rabbit IgG	- -	None AF532	AbCAM Thermo	Ab37994 A-11009	1:50 1:400
	IgA	-	AF555	Southern Biotech	1040-32	1:500
	EpCAM	G8.8	AF594	BioLegend	118222	1:400
	CD31	MEC13.3	AF647	BioLegend	102516	1:100
	Ki-67	B56	AF700	BD Biosciences	561277	1:50
3	CD45	30-F11	BV421	BioLegend	103134	1:100
	CD11b	5C6	FITC	Bio-Rad	MCA711F	1:100
	JOJO-1	-	AF532	Thermo	J11372	1:20,000
	Lyve-1	ALY7	eF570	Thermo	41-0443-82	1:100
	EpCAM	G8.8	AF594	BioLegend	118222	1:400
	CD11c	N418	AF647	BioLegend	117312	1:100
	MHC-II	M5/114.15.2	AF700	BioLegend	107622	1:100

Liver: 18 parameters, 4 cycles

Cycle	Marker	Clone	Conjugate	Vendor	Catalog Number	Dilution
1	CD4	GK1.5	BV421	BioLegend	100443	1:200
	Autofluorescence	-	BV510*	-	-	-
	Autofluorescence	-	AF488**	-	-	-
	LysM-tdTomato*	-	565-595 nm	-	-	-
	Laminin 1 + 2 Goat anti-rabbit IgG	- -	None AF594	AbCAM Thermo	Ab7463 A-11037	1:100 1:400
	E-cadherin	DECMA-1	AF647	BioLegend	147308	1:100
2	CD8	53-6.7	BV421	BioLegend	100738	1:200
	Autofluorescence	-	BV510*	-	-	-
	Autofluorescence	-	AF488**	-	-	-
	Desmin Goat anti-rabbit IgG Fab_2	- -	None AF532	AbCAM Thermo	Ab15200 Z25303	1:200 -
	Laminin 1 + 2 Goat anti-rabbit IgG	- -	None AF594	AbCAM Thermo	Ab7463 A-11037	1:100 1:400
	CXCR6	221002	AF647	Novus	FAB2145R	1:50
	CD44	IM7	AF700	BioLegend	103026	1:50
3	NK1.1	PK136	BV421	BioLegend	108731	1:50
	Autofluorescence	-	BV510*	-	-	-
	Autofluorescence	-	AF488**	-	-	-
	CD3	17A2	AF532	Thermo	58-0032-80	1:50
	Laminin 1 + 2	-	None	AbCAM	Ab7463	1:100

	Goat anti-rabbit IgG	-	AF594	Thermo	A-11037	1:400
	B220	RA3-6B2	AF647	BioLegend	103226	1:400
	CD45	30-F11	AF700	BioLegend	103128	1:50
4	Tim-4	21H12	BV421	BD Biosciences	742773	1:100
	Autofluorescence	-	BV510*	-	-	-
	CD11b	M1/70	AF488	BioLegend	101217	1:100
	Glutamine Synthetase Goat anti-rabbit IgG Fab_2	- -	None AF532	AbCAM Thermo	Ab49873 Z25303	1:200 -
	CD1d	1B1	PE	BD Biosciences	553846	1:100
	Laminin 1 + 2 Goat anti-rabbit IgG	- -	None AF594	AbCAM Thermo	Ab7463 A-11037	1:100 1:400
	CD11c	N418	AF647	BioLegend	117312	1:100
	MHC-II	M5/114.15.2	AF700	BioLegend	107622	1:100

*LsyM-tdTomato reporter animal

Naïve and immunized LNs: 41 parameters, 10 cycles

Cycle	Marker	Clone	Conjugate	Vendor	Catalog Number	Dilution
1	PD-1	29F.1.A12	BV421	BioLegend	135218	1:100
	CD35	8C12	BV510	BD Biosciences	740132	1:500
	B220	RA3-6B2	AF488	BD Biosciences	557669	1:400
	JOJO-1	-	-	Thermo	J11372	1:20,000
	CD3	17A2	AF594	BioLegend	100240	1:100
	Bcl6	K112-91	AF647	BD Biosciences	561525	1:50
	Ki-67	B56	AF700	BD Biosciences	561277	1:50
2	CD200	OX-90	BV421	BD Biosciences	565547	1:50
	αSMA	1A4	AF488	Thermo	53-9760-80	1:200
	JOJO-1	-	-	Thermo	J11372	1:20,000
	Lyve-1	ALY7	eF570	Thermo	41-0443-82	1:100
	CD3	17A2	AF594	BioLegend	100240	1:100
	gp38 Goat anti-hamster IgG	8.1.1 -	- AF647	BioLegend Thermo	127401 A-21451	1:50 1:400
	Collagen IV Goat anti-rabbit IgG	- -	- AF700	AbCAM Thermo	19808 A-21038	1:200 1:400
3	F4/80	BM8	BV421	BioLegend	123132	1:50
	CD11b	5C6	FITC	Thermo	MA5-16529	1:100
	JOJO-1	-	-	Thermo	J11372	1:20,000
	CD207	eBioL31	PE	Thermo	12-2075-80	1:50
	CD3	17A2	AF594	BioLegend	100240	1:100
	CD11c	N418	AF647	BioLegend	117312	1:100
4	CD8	53-6.7	BV421	BioLegend	100738	1:200
	JOJO-1	-	-	Thermo	J11372	1:20,000
	CD4	GK1.5	PE	BD Biosciences	553730	1:200
	CD3	17A2	AF594	BioLegend	100240	1:100
	Foxp3	FJK-16s	eF660	Thermo	50-5773-82	1:50
5	CD206	C068C2	BV421	BioLegend	141717	1:100
	SIRPα	P84	AF488	BioLegend	144024	1:50
	JOJO-1	-	-	Thermo	J11372	1:20,000
	TCRγδ	GL3	PE	BioLegend	118108	1:100
	CD3	17A2	AF594	BioLegend	100240	1:100
	DEC205	NLDC-145	AF647	BioLegend	138204	1:50
6	CD68	FA-11	BV421	BioLegend	137017	1:200
	JOJO-1	-	-	Thermo	J11372	1:20,000
	CD169	3D6.112	PE	Biolegend	142404	1:300
	CD3	17A2	AF594	BioLegend	100240	1:100
	CD64	X54-5/7.1	AF647	BioLegend	139322	1:50
7	CD21	7E9	Pacific Blue	BioLegend	123413	1:200
	CD106	429	AF488	BioLegend	105710	1:50
	JOJO-1	-	-	Thermo	J11372	1:20,000
	CD31	MEC13.3	PE	BD Biosciences	553373	1:200
	CD3	17A2	AF594	BioLegend	100240	1:100
	CD23	B3B4	AF647	BioLegend	101611	1:50
8	CD138	281-2	BV421	BD Biosciences	562610	1:50
	IRF4	3E4	FITC	Thermo	11-9858-82	1:50
	JOJO-1	-	-	Thermo	J11372	1:20,000
	SiglecF	E50-2440	PE	BD Biosciences	552126	1:100
	CD3	17A2	AF594	BioLegend	100240	1:100
	Pax5	1H9	AF647	BioLegend	649704	1:100
9	NK1.1	PK136	BV421	BioLegend	108731	1:50
	KLRG1	2F1	AF488	BD Biosciences	561619	1:56
	JOJO-1	-	-	Thermo	J11372	1:20,000
	GL-7	GL7	PE	BD Biosciences	561530	1:100
	CD3	17A2	AF594	BioLegend	100240	1:100
	CD44	IM7	AF647	BioLegend	103018	1:100
10	MHC-II	M5/114.15.2	BV421	BioLegend	107631	1:400
	IgD	11-26c.2a	AF488	BioLegend	405718	1:400
	JOJO-1	-	-	Thermo	J11372	1:20,000
	CD3	17A2	AF594	BioLegend	100240	1:100
	CD45	30-F11	AF647	BioLegend	103124	1:400

Table S3. IBEX panels for human LNs (See Fig. 5, Movie S8).

Metastatic pancreatic LN: 17 parameters, 4 cycles

Cycle	Marker	Clone	Conjugate	Vendor	Catalog Number	Dilution
1	Hoechst	-	-	Biotium	40046	1:5000
	CD8	SK1	AF488	BioLegend	344716	1:50
	CD3	UCHT1	AF532	Thermo	58-0038-42	1:50
	FOXP3	236A/E7	eF570	Thermo	41-4777-82	1:50
	EpCAM	9C4	AF594	BioLegend	324228	1:500
	CD25	M-A251	AF647	BioLegend	356127	1:50
	CD4	RPA-T4	AF700	BioLegend	300526	1:25
2	Hoechst	-	-	Biotium	40046	1:5000
	CD45	HI30	AF532	Thermo	58-0459-41	1:50
	PD-1	EH12.2H7	PE	BioLegend	329906	1:200
	EpCAM	9C4	AF594	BioLegend	324228	1:500
	CD69	FN50	AF647	BioLegend	310918	1:100
3	Hoechst	-	-	Biotium	40046	1:5000
	HLA-DR	L243	AF488	BioLegend	307619	1:200
	SPARC	Goat IgG	AF532	R&D	AF941 (Unconjugated)	1:50
	EpCAM	9C4	AF594	BioLegend	324228	1:500
	CD68	KP1	AF647	Santa Cruz	Sc-200060	1:100
	Collagen IV Goat anti-rabbit IgG	- -	None AF700	AbCAM Thermo	Ab6586 A-21038	1:200 1:400
4	Hoechst	-	-	Biotium	40046	1:5000
	CD21	Bu32	AF532	BioLegend	Custom	1:400
	EpCAM	9C4	AF594	BioLegend	324228	1:500
	CD138	MI15	AF647	BioLegend	356523	1:200
	Ki-67	B56	AF700	BD Biosciences	561277	1:50

Mesenteric LN: 66 parameters, 20 cycles

Cycle	Marker	Clone	Conjugate	Vendor	Catalog Number	Dilution
1	Hoechst	-	-	Biotium	40046	1:5000
	CD20	L26	AF488	Thermo	53-0202-82	1:200
	SPARC	Goat IgG	AF532	R&D	AF941 (Unconjugated)	1:50
	CD10	FR4D11	PE	Caprico Biotechnologies	103926	1:50
	CD3	UCHT1	AF594	BioLegend	300446	1:100
	BCL2	100	AF647	BioLegend	658705	1:25
	Collagen IV Goat anti-rabbit IgG	- -	None AF700	AbCAM Thermo	Ab6586 A-21038	1:200 1:400
2	Hoechst	-	-	Biotium	40046	1:5000
	IgD	IA6-2	AF488	BioLegend	348216	1:25
	CD21	Bu32	AF532	BioLegend	NA, Custom	1:600
	CD138	MI15	PE	BioLegend	356504	1:200
	CD3	UCHT1	AF594	BioLegend	300446	1:100
	BCL6	K112-91	AF647	BD Biosciences	561525	1:25
	CD31	WM59	AF700	BioLegend	303133	1:25
3	Hoechst	-	-	Biotium	40046	1:5000
	HLA-DR	L243	AF488	BioLegend	307620	1:100
	CD23	EBVCS-5	AF532	BioLegend	NA, Custom	1:25
	CD1c	L161	PE	BioLegend	331506	1:50
	CD3	UCHT1	AF594	BioLegend	300446	1:100
	CD163	GH1/61	AF647	BioLegend	333620	1:100
	CD11c	B-Ly6	AF700	BD Biosciences	561352	1:25
4	Hoechst	-	-	Biotium	40046	1:5000
	CD8	SK1	AF488	BioLegend	344716	1:25
	CD4	RPA-T4	AF532	Thermo	58-0049-42	1:25
	FOXP3	236A/E7	eF570	Thermo	41-4777-82	1:25
	CD3	UCHT1	AF594	BioLegend	300446	1:100
	CD25	M-A251	AF647	BioLegend	356128	1:50
	Ki-67	B56	AF700	BD Biosciences	561277	1:50
5	Hoechst	-	-	Biotium	40046	1:5000
	ICOS	CS98.4A	AF488	BioLegend	313514	1:25
	CXCL13	Goat IgG	AF532	R&D	AF801 (Unconjugated)	1:25
	PD-1	EH12.2H7	PE	BioLegend	329906	1:100
	CD3	UCHT1	AF594	BioLegend	300446	1:100
	CD69	FN50	AF647	BioLegend	310918	1:25
6	Hoechst	-	-	Biotium	40046	1:5000
	CD117	104D2	AF488	BioLegend	313234	1:50
	Lyve-1	Goat IgG	AF532	R&D	AF2089 (Unconjugated)	1:100

	CD35	E11	PE	BioLegend	333406	1:800
	CD3	UCHT1	AF594	BioLegend	300446	1:100
	CD68	KP1	AF647	Santa Cruz	sc-20060	1:100
	CD38	HIT2	AF700	BioLegend	303524	1:25
7	Hoechst	-	-	Biotium	40046	1:5000
	Clec9a	8F9	AF488	BioLegend	Custom	1:25
	Tim-3	344823	AF532	R&D	MAB2365 (Unconjugated)	1:25
	IRF4	IRF4.3E4	PE	BioLegend	646404	1:25
	CD3	UCHT1	AF594	BioLegend	300446	1:100
	DC-SIGN	9E9A8	AF647	BioLegend	330112	1:50
8	Hoechst	-	-	Biotium	40046	1:5000
	CXCL12	79018	AF532	R&D	MAB350-500 (Unconjugated)	1:25
	TCRγδ	B1	PE	BioLegend	331210	1:100
	CD3	UCHT1	AF594	BioLegend	300446	1:100
	Vα7.2	3C10	AF647	BioLegend	351726	1:50
9	Hoechst	-	-	Biotium	40046	1:5000
	α-SMA	1A4	AF488	Thermo	53-9760-82	1:100
	CD45	HI30	AF532	Thermo	58-0459-42	1:25
	CD106	STA	PE	BioLegend	305806	1:50
	CD3	UCHT1	AF594	BioLegend	300446	1:100
	CD44	IM7	AF647	BioLegend	103018	1:50
10	Hoechst	-	-	Biotium	40046	1:5000
	Lumican	Goat IgG	AF532	R&D	AF2745 (Unconjugated)	1:50
	CD34	QBEND/10	PE	Thermo	MAI-10205	1:50
	CD3	UCHT1	AF594	BioLegend	300446	1:100
	CD54	HA58	AF647	BioLegend	353114	1:50
11	Hoechst	-	-	Biotium	40046	1:5000
	NF-H/NF-M	SM1-35	AF488	BioLegend	835614	1:50
	CD3	UCHT1	AF594	BioLegend	300446	1:100
	CD66b	G10F5	AF647	BioLegend	305110	1:25
12	Hoechst	-	-	Biotium	40046	1:5000
	CD166	EPR2759	AF488	AbCAM	Ab197543	1:125
	Fibronectin	2F4	AF532	Novus	NBP2-22113AF532	1:25
	CD39	A1	PE	BioLegend	328208	1:50
	CD3	UCHT1	AF594	BioLegend	300446	1:100
	Cytokeratin	AE1/AE3	eF660	Thermo	50-9003-82	1:100
13	Hoechst	-	-	Biotium	40046	1:5000
	MARCO Zenon Fab	Rabbit IgG -	- AF532	Thermo Thermo	PA5-64134 Z25303	1:25 NA
	CD94	DX22	PE	BioLegend	305506	1:50
	CD3	UCHT1	AF594	BioLegend	300446	1:100
	EpCAM	9C4	AF647	BioLegend	324212	1:100
14	Hoechst	-	-	Biotium	40046	1:5000
	β-Tubulin 3	TUJ1	AF532	BioLegend	Custom	1:50
	CD49a	TS2/7	PE	BioLegend	328304	1:50
	CD3	UCHT1	AF594	BioLegend	300446	1:100
	IgM	EPR5539-65-4	AF647	AbCAM	Ab200629	1:100
15	Hoechst	-	-	Biotium	40046	1:5000
	IgA2	A9604D2	AF488	SouthernBiotech	9140-30	1:500
	p53	PAb 240	PE	Novus	NB200-103PE	1:50
	CD3	UCHT1	AF594	BioLegend	300446	1:100
	IgA1	B3506B4	AF647	SouthernBiotech	9130-31	1:500
16	Hoechst	-	-	Biotium	40046	1:5000
	Laminin 1+2 Zenon Fab	Rabbit IgG -	- AF488	AbCAM Thermo	Ab7463 Z25302	1:100 NA
	Lysozyme Zenon Fab	Rabbit IgG -	- AF532	AbCAM Thermo	Ab2408 Z25303	1:50 NA
	CD3	UCHT1	AF594	BioLegend	300446	1:100
17	Hoechst	-	-	Biotium	40046	1:5000
	Keratin 18	1G11C4	CoraLite488	ProteinTech	CL488-66187	1:50
	Vimentin	O91D3	AF532	BioLegend	Custom	1:200
	CD3	UCHT1	AF594	BioLegend	300446	1:100
18	Hoechst	-	-	Biotium	40046	1:5000
	Desmin	Y66	AF488	AbCAM	Ab185033	1:200
	CD3	UCHT1	AF594	BioLegend	300446	1:100
	Tryptase Zenon Fab	AA1 -	- AF700	AbCAM Thermo	Ab2378 Z25011	1:50 NA
19	Hoechst	-	-	Biotium	40046	1:5000
	Donkey anti-goat IgG	-	AF488	Thermo	A11055	1:1000
	CD45	F10-89-4	PE/iFluor594	Caprico Biotechnologies	1016185	1:50
	CD3	UCHT1	AF594	BioLegend	300446	1:100
	Donkey anti-rabbit IgG	-	AF647	Thermo	A31573	1:1000
20	Hoechst	-	-	Biotium	40046	1:5000
	Keratin 14 Donkey anti-chicken IgY	Poly9060 -	- FITC	BioLegend Thermo	906004 SA1-72000	1:50 1:200
	CD3	UCHT1	AF594	BioLegend	300446	1:100

	Goat anti-rat IgG	-	AF647	Thermo	A21247	1:1000

Table S4. Reagents used for multi-plex Opal IHC experiments (See Figs. 6B, S7A, and Movie S9).

Marker	Clone	Conjugate	Vendor	Cat No.	Isotype	Dilution	Time to bleach with $LiBH_4$
CD3e	D4V8L	None	CST	99940	Rabbit IgG	1:100	-
CD4	D7D2Z	None	CST	25229	Rabbit IgG	1:100	-
CD8	D4W2Z	None	CST	98941	Rabbit IgG	1:200	-
CD11c	D1V9Y	None	CST	97585	Rabbit IgG	1:100	-
CD19	D4V4B	None	CST	90176	Rabbit IgG	1:300	-
CD138	281-2	PE	BioLegend	142504	Rat IgG2a, κ	1:100	-
Collagen IV	-	None	AbCam	19808	Rabbit IgG	1:50	-
CXCL9	-	None	R&D	AF-492-NA	Goat IgG	1:50	-
E-cadherin	DECMA-1	AF488	Thermo	53-3249-82	Rat IgG1, κ	1:100	-
F4/80	D2S9R	None	CST	70076	Rabbit IgG	1:100	-
F4/80	BM8	BV421	BioLegend	123132	Rat IgG2a, κ	1:50	-
Foxp3	D6O8R	None	CST	12653	Rabbit IgG	1:200	-
Laminin	-	None	AbCam	Ab7463	Rabbit IgG	1:100	-
MHCII	-	None	AbCam	Ab180779	Rabbit IgG	1:100	-
Anti-rabbit IgG		HRP			Goat IgG	1:5	-
-	-	Opal 520	Akoya Biosciences	FP1487001KT	-	-	>30 minutes
-	-	Opal 540	Akoya Biosciences	FP1494001KT	-	-	>30 minutes
-	-	Opal 570	Akoya Biosciences	FP1488001KT	-	-	30 minutes
-	-	Opal 620	Akoya Biosciences	FP1495001KT	-	-	>30 minutes
-	-	Opal 650	Akoya Biosciences	FP1496001KT	-	-	30 minutes
-	-	Opal 690	Akoya Biosciences	FP1497001KT	-	-	30 minutes

Table S5. Reagents used in combined IBEX oligonucleotide-based staining panel. (See Figs. 6D, S7C-D, and Movie S9).

Cycle	Antibody/Dye	Clone	Vendor	Cat No.	Imaging oligo sequence
1	Hoechst	-	Biotium	40046	-
	SIRPα AF488	P84	BioLegend	144024	-
	Foxp3 AF532	FJK-16s	Thermo	58-5773-82	-
	CD31 PE	MEC13.3	BD Biosciences	553373	-
	CD11c AF647	N418	BioLegend	117312	-
	Ki-67 AF700	B56	BD Biosciences	561277	-
2	Hoechst	-	Biotium	40046	-
	CD169 AF532*	3D6.112	BioLegend	142425	ATGACTGTCGTCAATTG
	IgD Atto 550*	11.26c.2a	BioLegend	405745	GGACAACGGATATGATG
	CD11b AF647*	M1/70	BioLegend	101265	ACAAATGAGCCTTCATG
	MHCII IR700*	M5/114.15.2	BioLegend	107653	ATCATACTGGTGACCTG
3	Hoechst	-	Biotium	40046	-
	CD45 AF532*	30-F11	BioLegend	103159	TCTGCTCCATAGCCATG
	CD68 Atto 550*	FA-11	BioLegend	137031	TCCCGTGAAAGAAAGTG
	CD3 AF647*	17A2	BioLegend	100251	ATCGAGCGGACATACTG
Non-IBEX**	B220 AF488*	RA3-6B2	BioLegend	103263	ATTATGAGGTGTAGGTG
	CD11c AF594*	N418	BioLegend	117355	GCAAGCGTCCATAACTG

*Denotes fluorescent label provided by complementary fluorescent oligonucleotides.

**Additional reagents tested (Figure S7C).

Movies S1-S9 Legends

Movie S1. High dimensional imaging of the spleen using IBEX. Confocal images of mouse spleen tissue from a 3 cycle 16 parameter IBEX experiment with CD4 serving as a fiducial. See Fig. 3. Data are representative of 2 similar experiments.

Movie S2. High dimensional imaging of the thymus using IBEX. Confocal images of mouse thymus tissue from a 5 cycle 26 parameter IBEX experiment with CD3 serving as a fiducial. See Fig. 3. Data are representative of 2 similar experiments.

Movie S3. High dimensional imaging of the lung using IBEX. Confocal images of mouse lung tissue from a 4 cycle 23 parameter IBEX experiment with CD31 serving as a fiducial. See Fig. 3. Data are representative of 2 similar experiments.

Movie S4. High dimensional imaging of the small intestine using IBEX. Confocal images of mouse small intestine tissue from a 3 cycle 20 parameter IBEX experiment with EpCAM serving as a fiducial. See Fig. 3. Data are representative of 2 similar experiments.

Movie S5. High dimensional imaging of the liver using IBEX. Confocal images of liver tissue from a LysM-tdTomato mouse. A 4 cycle 18 parameter IBEX experiment was performed with Laminin serving as a fiducial. See Fig. 3. Data are representative of 2 similar experiments.

Movie S6. High dimensional imaging of naïve and immunized LNs using IBEX. Confocal images of pLNs from naïve and SRBC-immunized mice from 10 cycle 41 parameter IBEX experiments. See Fig. 4A. Data are representative of 2 similar experiments.

Movie S7. Comparable staining observed by serial and iterative immunofluorescence methods. Confocal images of inguinal LN (iLN) or pLNs from SRBC-immunized mice demonstrating qualitatively similar staining patterns when antibody panels were applied on individual sections alone (serial) versus on the same section iteratively (IBEX). See Figs. 4 and S5. Data are representative of 2 similar experiments.

Movie S8. IBEX scales to capture ultra-high content imaging in large human tissues. Confocal images of human LN tissue section with metastatic lesions from a 4 cycle 17 parameter IBEX experiment or human mesenteric LN from a 20 cycle 66 parameter IBEX experiment. See Fig. 5. Data are representative of similar experiments in normal and diseased human LNs.

Movie S9. Extensions of IBEX workflow to include Opal fluorophores and oligo-conjugated antibodies. Representative confocal images from a 10 parameter 4 cycle IBEX experiment incorporating Opal fluorophores performed on heavily fixed mouse pLN tissue sections. Confocal

images from a 13 parameter 3 cycle IBEX experiment performed on mouse inguinal LN sections. Markers were visualized using either fluorescently-conjugated antibodies (Cycle 1) or oligo-conjugated antibodies and complementary fluorescent oligos (Cycles 2-3). See Figs. 6 and S7. Data are representative of 2-4 similar experiments.

References

1. K. Mao *et al.,* Innate and adaptive lymphocytes sequentially shape the gut microbiota and lipid metabolism. *Nature* **554**, 255-259 (2018).
2. A. Gola et al., Prime and target immunization protects against liver-stage malaria in mice. *Sci. Transl. Med.* **10**, 460 (2018).
3. T.Z. Veres et al., Allergen-induced CD4+ T cell cytokine production within airway mucosal dendritic cell-T cell clusters drives the local recruitment of myeloid effector cells. *J. Immunol.* **198**, 895-907 (2017).
4. M.Y. Gerner, W. Kastenmuller, I. Ifrim, J. Kabat, R.N. Germain, Histo-cytometry: a method for highly multiplex quantitative tissue imaging analysis applied to dendritic cell subset microanatomy in lymph nodes. *Immunity* **37**, 364-376 (2012).
5. I. Sayin *et al.,* Spatial distribution and function of T follicular regulatory cells in human lymph nodes. *J. Exp. Med.* **215**, 1531-1542 (2018).
6. J. Schindelin *et al.,* Fiji: an open-source platform for biological-image analysis. *Nat. Methods* **9**, 676-682 (2012).
7. Z. Wang, A.C. Bovik, H.R. Sheikh, E.P. Simoncelli, Image quality assessment: from error visibility to structural similarity. *IEEE Trans. Image Process* **13**, 600-612 (2004).
8. D. Schapiro *et al.*, histoCAT: analysis of cell phenotypes and interactions in multiplex image cytometry data. *Nat. Methods* **14**, 873-876 (2017).
9. S. Berg *et al.,* ilastik: interactive machine learning for (bio)image analysis. *Nat. Methods* **16**, 1226-1232 (2019).
10. A.E. Carpenter *et al.,* CellProfiler: image analysis software for identifying and quantifying cell phenotypes. *Genome Biol.* **7**, R100 (2006).
11. S. Anders, W. Huber, Differential expression analysis for sequence count data. *Genome Biol.* **11**, R106 (2010).
12. S.K. Saka *et al.,* Immuno-SABER enables highly multiplexed and amplified protein imaging in tissues. *Nat. Biotechnol.* **37**, 1080-1090 (2019).